2015

Thin Films of Gold Nanoparticles: Temporal Stability and Mechanisms of Degradation

Jeanne Xu
jxu3@wellesley.edu

Thin Films of Gold Nanoparticles: Temporal Stability and Mechanisms of Degradation

Jeanne J. Xu

Advisor: Dr. Nolan T. Flynn

Chemistry Department

Submitted as partial fulfillment of a Bachelor of Arts degree with honors in Chemistry at Wellesley College.

April 2015

Abstract

Thin films of gold nanoparticles (Au NPs) are of interest because of their unique physicochemical properties. These thin films have potential applications in electrical devices, chemical sensing, and biosensing. Retaining the integrity of the thin film is important for such applications. The purpose of this project is to assess the temporal stability and to explore the mechanisms of degradation of thin films of Au NPs on glass substrates. Thin films were fabricated through a layer-by-layer deposition process. Clean glass substrates were sequentially immersed in solutions of (3-aminopropyl)trimethoxysilane, synthesized Au NPs, and 1-dodecanethiol (DT). The wettability of each layer was characterized with contact angle goniometry. Upon the completion of thin film fabrication, slides were immersed in ultrapure water (nH_2O) and changes in wettability were observed over a 7-day period. Although thin films of gold had more hydrophobic surfaces than DT-containing controls lacking Au NPs, there was still a significant decrease in contact angle once the films were immersed in high purity water. Thin film degradation was quantified by a decrease in contact angle. Two possible mechanisms of thin film degradation were investigated: (1) the desorption of DT from thin films by oxidation and (2) the desorption of Au NPs from the thin films. Antioxidant was added to the storage solution to test the oxidation mechanism. Contact angle analysis was used to monitor the changes in wettability of thin films in nH_2O with antioxidant. The presence of antioxidant in nH_2O improved thin film integrity. Inductively coupled plasma atomic emission spectroscopy was used to determine the change in Au^{3+} concentration from day 0 and day 7. No substantial change in Au^{3+} was observed from day 0 to day 7. Between the two mechanisms that were explored, thin film degradation appeared to occur primarily by the oxidation of DT molecules and their desorption into the surrounding medium.

Acknowledgements

First and foremost, I would like to express my sincerest gratitude to my advisor, Nolan T. Flynn. Thank you for taking me under your wing and giving me this opportunity! I truly appreciated your guidance, encouraging words, sage wisdom, and humor throughout my research experience. Thank you for your infinite support and patience. My only regret is that I was never able to take a class with you.

I would also like to thank the members of my thesis committee: Michael Hearn, Nancy Mukundan, and Shiao-wei Tham. I appreciate your willingness to serve on my thesis committee and for sharing your insightful comments throughout this thesis experience.

To my fellow Flynn lab members: thank you for all the laughs, miseries, and memories we have shared together! Yuka Milton, thank you for mentoring me in the ways of the Flynn lab. To my fellow thesis-er Sara Musetti, thank you for your friendship and your endless support. To Amal Cheema, Elizabeth Durham, and Kathleen Chen, thank you all for bringing a good mix of sassiness and sweetness to the lab. Liz McLoughlin ‘14, thank you for the wisdom you have shared with me and I shall forever keep your quotes on the quote board from Summer 2014 near and dear to my heart. Though I have never met any of you, I have become very familiar with your lab notebooks so I would like to thank Ann Gaffey ‘06, Julia Lin ‘07, Alex Bear ‘09, Claire Rimkus ‘10, and Kristen Worthen (Cameron University) for your work on the thin film project!

To one of my dearest friends, a fellow thesis-er, a honorary Flynn lab member, and my lab buddy, Alice Liao, thank you for your friendship and everything you have done for me! From the countless hours we spent in lab together on the weekends trying to finish our experiments to the food outings we spontaneously decide on to treat ourselves or just to satisfy our cravings, I am thankful for these memories. To Angela Ai and Shirley Lu, who would have thought that after rooming together we would all thesis together? Thank you two for all the memories from first year to now! Also, special thanks to Angela for helping me edit my thesis. Ashley Gaing, my “twin,” I am very grateful to have met you! Your friendship means a lot to me despite me being “soulless and heartless.” I do hope you are able to navigate Boston by yourself by the time we graduate.

Frieda Zhang, you are inspirational and brilliant. Lynn Hsu, thank you for making sure that I eat my meals. Jane Zhu, Hannah Sim, and Kailin Ho, you three always bring a smile to my face. Jenny Chan, thank you for always checking up on me and making sure that I am well. Thank you all for your friendship and your support!

To my fellow chemistry and chemical physics thesis-ers, Aiman Sherani, Michelle Brann, Katherine Tran, and Ali Dunn, there were many long nights and many Starbucks runs, but we made it!

I would also like to acknowledge the Wellesley College Science Center and Staley Fund for Cancer Related Research for supporting this research.

Lastly, I would like to thank my family for their endless encouragement and support!

Table of Contents

1. Introduction

In December of 1959, a notable lecture titled "There is Plenty of Room at the Bottom" was given by physicist Richard Feynman.[1] Throughout the lecture he proposed various ideas illustrating the manipulation of matter at the atomic level. For example, Feynman suggested the possibility of arranging atoms in any way we want. This proposition became a reality on September 28th, 1989 when Don Eigler, an IBM physicist, became the first person to manipulate and move individual atoms. Shortly after this achievement, Eigler arranged xenon atoms to spell out "IBM".[2] Although Feynman's thought experiment was not well received at first, it can be said that the origin of nanotechnology started with this very lecture.

Nanotechnology began to garner scientific and commercial attention in the 1990s. Since then, there have been many advancements in the understanding and applications of nanoscience. Materials of size of the nanometer (10^{-9} m) scale exhibit characteristics and behaviors that are different from the properties of the same materials in bulk. In addition to the unique physicochemical properties of nanoscale materials, they are characterized by their high surface area to mass ratio. Therefore, nanomaterials are capable of interacting with more surrounding materials than larger-scale materials. These nanomaterials come in all shapes and sizes. Among the various types of nanomaterials, the nanoparticle is of immense interest for many reasons. For instance, the intrinsic properties of metal nanoparticles, such as optical, sensing, and catalytic properties, are dependent on its size and shape. Nanoparticles can also self-assemble and these assembled nanoparticles are capable of much more than their individual counterpart.[3] Upon self-assembly, the properties of the nanoparticles, such as plasmon, conductivity, color, and surface morphology, can change.[3] The ability to manipulate the properties of nanoparticles and their ability to assemble into more complex 1D, 2D, and 3D nanostructures can lead to the

development of many novel nanoparticle-based technologies with applications in medicine, sensors, and electronics.

1.1 Gold Nanoparticles

Among metal nanoparticles, gold nanoparticles, denoted as Au NPs hereafter, are of particular interest because of their stability and their tunable optical and electrochemical properties.[4] In addition, Au NPs are very biocompatible and have been utilized in many biomedical applications, such as diagnostic tests, cancer therapy, and drug delivery.[5,6]

1.1.1 Gold Nanoparticles as Sensors

Gold nanoparticles have been considered and employed in sensing applications because of their unique optical properties. The underlying principle behind many color-based sensors relies on an important property of Au NPs – their surface plasmon resonance (SPR), which is attributed to the oscillation of electrons on the particle surface.[7] As reported by Sperling et al., Au NPs that are between 4–40 nm in diameter exhibit characteristic absorption or SPR peaks between 510–530 nm.[6] The basis of colorimetric detection of analytes relies on the change of the SPR peak, which can be attributed to the analyte binding to the particle surface or caused by changes in the spatial distance between Au NPs.[8] Ferhan et al. developed a gold nanoparticle-based colorimetric sensor for lead detection.[9] Gold nanoparticles functionalized with thiolsulfate were loaded onto a glass substrate modified with poly(oligo(ethylene glycol) methacrylate (POEGMA) brushes.

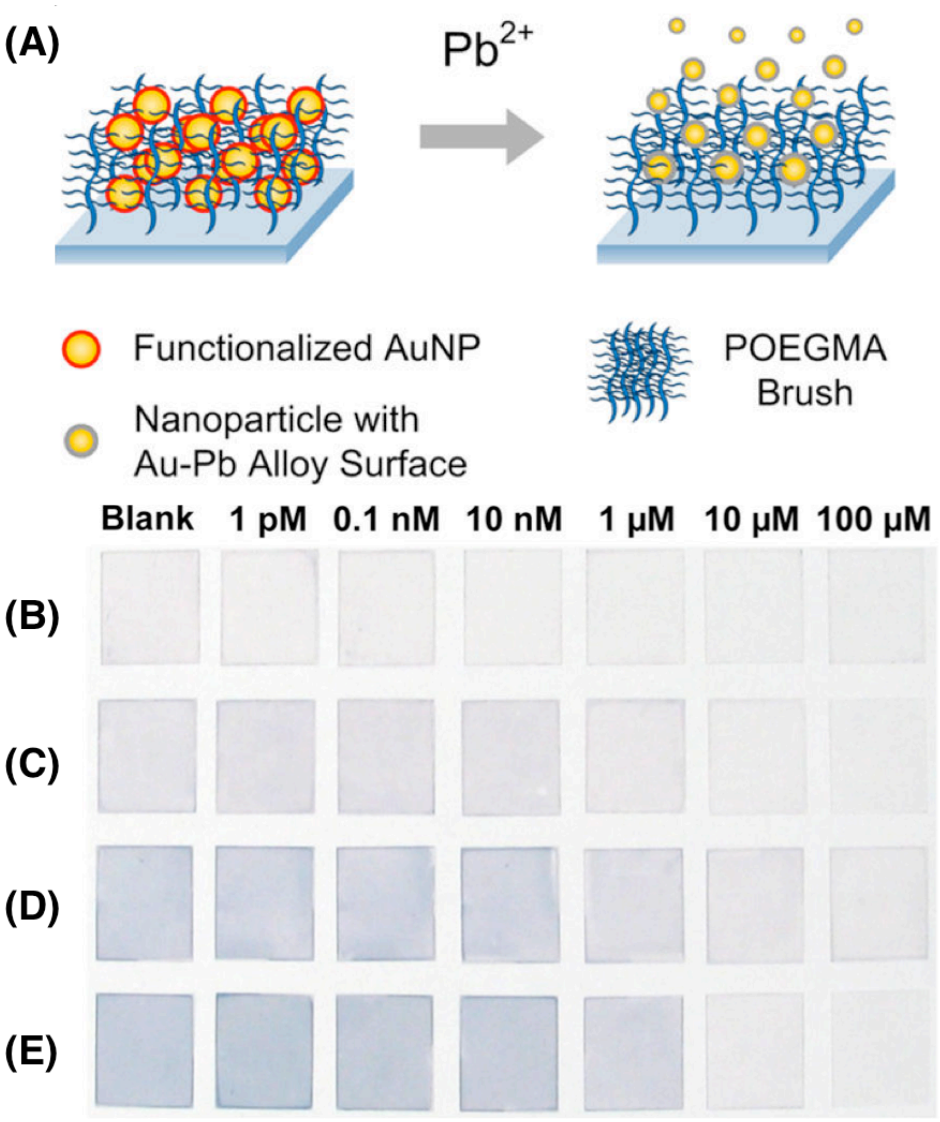

Figure 1. (A) Schematic of Au NP-based colorimetric sensor for lead detection. Glass coverslips treated with **(B)** (3-aminopropyl)triethoxysilane (APTS) served as a control. Glass coverslips treated with POEGMA for **(C)** 1 hour, **(D)** 3 hours, and **(E)** 6 hours. The glass coverslips were then immersed in 0 M (blank), 1 pM, 0.1 nM, 10 nM, 1 µM, 10 µM, and 100 µM Pb^{2+} solution. Adapted from Ferhan et al.[9]

As illustrated in Figure 1, the fabricated sensors resulted in a bluish color. In the presence of lead (II) ions and 2-mercaptoethanol, Au-Pb alloys were formed and released from the POEGMA brushes. A loss of color was observed as the concentration of Pb^{2+} increased. Biosensors employing the aggregation principle of Au NPs have also been developed because of color changes that accompany Au NP aggregation. Wang et al. were able to detect hydrogen peroxide

(H_2O_2) by using cysteine to mediate Au NP aggregation.[10] Figure 2 shows the cysteine-mediated aggregation of Au NPs through interparticle H-bond formation and electrostatic interactions.

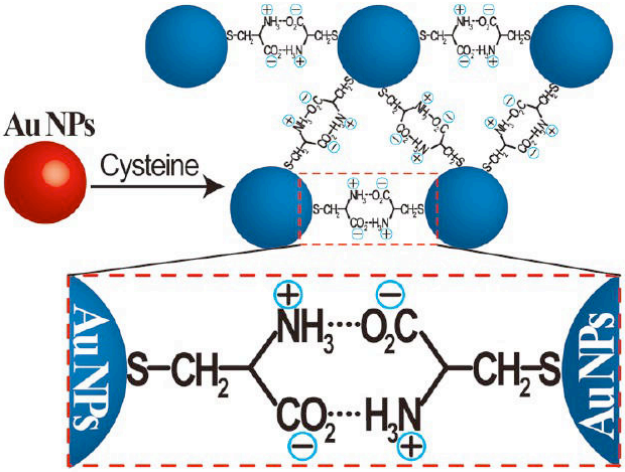

Figure 2. Schematic cysteine-mediated aggregation of Au NPs. Adapted from Wang et al.[10]

A system based on the inhibition of cysteine-mediated Au NP aggregation, the iodide ion-catalyzed oxidation of cysteine by H_2O_2 to cystine, was employed for H_2O_2 and glucose sensing. Wang and colleagues used this system to study the biocatalyzed oxidation of glucose by glucose oxidase, GOx, which yields gluconic acid and H_2O_2. With the cysteine/I^-/Au NP reporter system, H_2O_2 concentration could be determined by monitoring the Au NP aggregation or lack of Au NP aggregation. In addition, glucose concentration can be obtained because the concentration of glucose controls the concentration of H_2O_2. These sensors have the potential to monitor glucose levels in saliva.

1.1.2 Surface-enhanced Raman Spectroscopy

The surface plasmon resonance of gold nanoparticles plays an integral part in surface-enhanced Raman spectroscopy (SERS). Raman scattering, the inelastic scattering of photons, is significantly enhanced near a gold surface because of the excitation of localized surface plasmons. This allows for better detection of the analyte since the detection signal is amplified.

Lv and colleagues used a nanostructured Au coated indium tin dioxide (ITO) electrode to detect multidrug-resistant bacteria, such as *Escherichia coli* and *Staphylococcus aureus*.[11] Doxorubicin, an anthracycline antibiotic agent that inhibits growth of *E. coli* and *S. aureus* upon binding, is used to modify the Au NPs. SERS can be used to study the specific binding behavior of doxorubicin with the target bacteria to provide more insight on the physicochemical characterization of microorganisms. In addition, the nanostructured Au modified ITO electrode with doxorubicin can be used to rapidly detect bacteria with high sensitivity.

1.1.3 Self-assembled Monolayers

Self-assembled monolayers (SAMs) are spontaneous molecular assembles of organic molecules on solid surfaces formed through adsorption.[12] Two key physical characteristics determine the structure of SAMs: geometric shape and radius of curvature. Although one may envision gold nanoparticles to be perfect spheres, Au NPs larger than 0.8 nm in diameter often exhibit a truncated octahedral geometry (Figure 3).

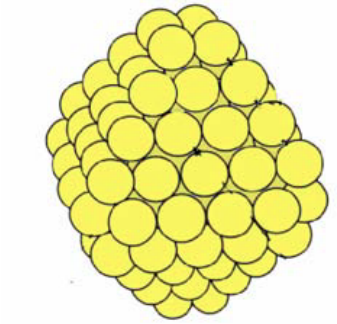

Figure 3. Gold nanoparticle with a truncated octahedral geometry. Adapted from Love et al.[12]

Therefore, small gold nanoparticles have high radii of curvature. The molecules that self-assemble have a headgroup with an affinity for the substrate. Sometimes at the other terminus of the molecule, another headgroup is present for the formation of another SAM on top of it.

Mamun et al. investigated the effect of identical terminal groups but different molecular structures on SAM surfaces.[13] They decided to examine two molecules: 1-dodecanethiol (DT) and 4-methylbenzenethiol (MBT) (Figure 4).

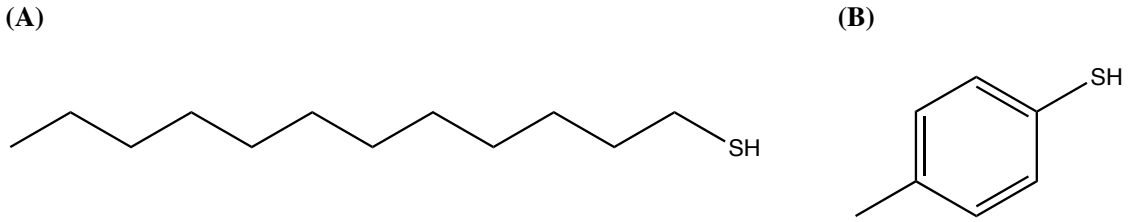

Figure 4. Chemical structures of **(A)** 1-dodecanethiol and **(B)** 4-methylbenzenethiol.

Surface morphology was characterized by surface geometry and nanoscale surface roughness. The DT-SAM surface was deemed to be more corrugated than the MBT-SAM surface. Therefore, the surface morphology for Au NP adsorption on the DT-SAM surface was non-uniform and resulted in the aggregation of Au NPs. On the other hand, the MBT-SAM surface was smoother, which allowed for a more uniform dispersion of Au NPs across the surface. In addition, they found that nanoscale surface roughness increased hydrophobicity of the surface.

Self-assembled monolayers (SAMs) are attractive because they provide a means for modifying the chemical composition and structures of surfaces through functionalization of the monolayer's terminal groups. In addition, SAMs are relatively easy to prepare and they provide chemical stability.

1.2 Gold Nanoparticle Thin Films

Although gold nanoparticles are very capable as sensors, immobilizing gold nanoparticles to form a thin film on a substrate can provide better stability.[8] The properties of the thin film can be adjusted depending on which parameters are investigated and optimized. The effect of annealing time (at 220 °C) and film thickness of dodecanethiol encapsulated Au NP Langmuir-Schafer thin films on its optical properties was investigated by Abbas and colleagues.[7] In their

work they found that different annealing times resulted in changes in thin film morphology, especially in thin films with more layers. In addition, they found that the surface plasmon resonance (SPR) peak of thin films of all thicknesses became sharper. For all thicknesses, after 30 minutes of annealing, the SPR peaks experienced a redshift, which was followed by a blue shift after an hour of annealing.

1.2.1 Deposition Methods

Thin films of gold nanoparticles can be fabricated by many different deposition methods, such as layer-by-layer, spin coating, and other techniques shown in Figure 5.[7,14]

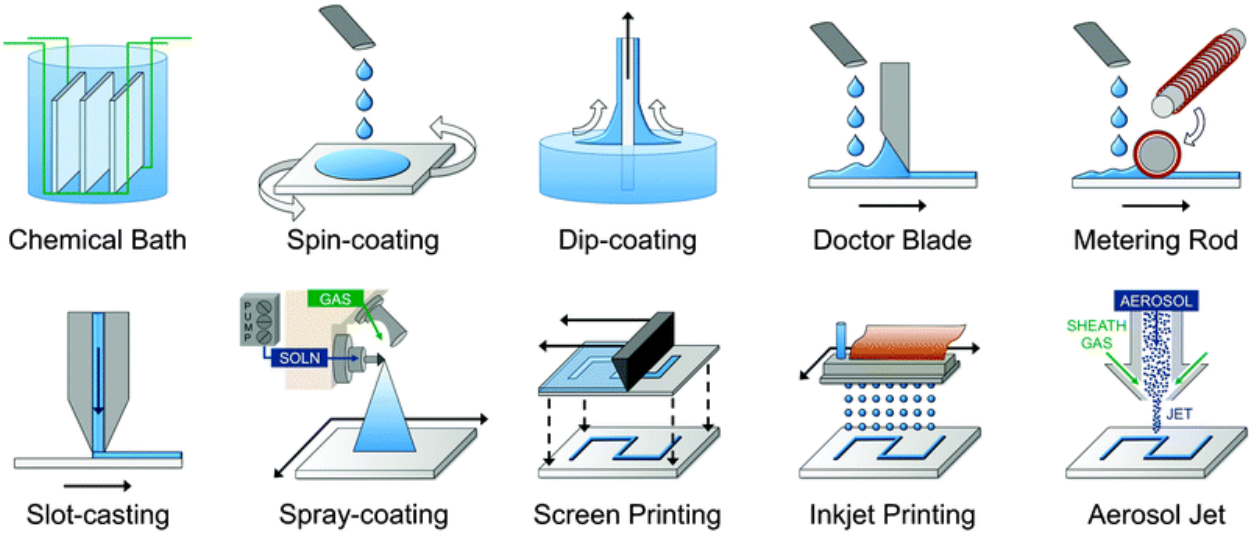

Figure 5. Various solution deposition techniques for thin film fabrication. Figure taken from Pasquarelli et al.[14]

The layer-by-layer immersion method is employed in this research. The substrate is immersed sequentially in a series of solutions that make up the components of the thin film. Spin coating is another fairly simple deposition technique. A small drop of coating material is dropped onto the substrate surface. Then the instrument uses centrifugal force to spread the coating material. Abbas et al. used the Langmuir-Schaefer deposition technique to form the their Au NP thin films.[7] In this deposition method, one or more monolayers of molecules are deposited onto the solid substrate from a liquid surface by horizontal dipping rather than by vertical dipping. Thin

films obtained can be highly organized ranging from a very thin monolayer to multilayer structures consisting of hundreds of monolayers.

1.2.2 Characterization Techniques

1.2.2.1 Dynamic Light Scattering

Both hydrodynamic diameter and uniformity of size distribution can be characterized with dynamic light scattering (DLS). In this technique, particle size is related to Brownian motion, the random movement of particles in a suspension because of collisions with molecules of the surrounding medium.[15] The relationship between the velocity of a particle in solution and its hydrodynamic radius can described by the Stokes-Einstein equation (Eq. 1), where D_h is the hydrodynamic diameter, D is the translational diffusion coefficient, k is the Boltzmann's constant, T is the absolute temperature, and η is the viscosity.

$$D_h = \frac{kT}{3\pi\eta D} \quad (1)$$

The size of the particles is determined by fluctuations in the intensity of light scattered by the sample. A laser illuminates a solution of analyte, and the rate at which the intensity of scattered light fluctuates is measured as a function of time. Since the rate of the intensity fluctuations is dependent on the how fast the particles are moving, particle size can be inferred, as smaller particles will have faster rates than larger particles. van der Zande et al. monitored particle size and aggregation of colloidal gold rods with DLS.[16] Mohr et al. used DLS to detect aggregation of liposomes modified with a hyperbranched polyglycerol lipid.[17]

1.2.2.2 Contact Angle Goniometry

Contact angle goniometry, illustrated in Figure 6, is used to quantify the wettability (hydrophobicity or hydrophilicity) of a solid surface. The goniometer dispenses a water droplet onto the surface of a solid substrate. The static or equilibrium contact angle (θ) is dependent on

the intermolecular interactions among the liquid, vapor, and solid phases. As a result the contact angle is the angle where the liquid and the vapor interfaces meets the solid surface.

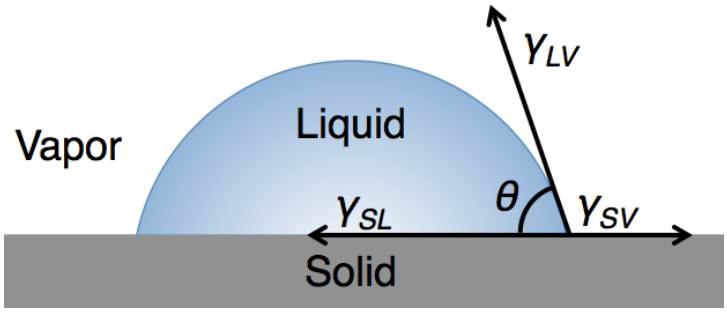

Figure 6. Schematic of a sessile drop on a solid surface with static contact angle.

The contact angle (θ) of a sessile drop on a solid substrate can be predicted from Young's equation (Eq. 2), where γ_{LV} is the liquid-vapor interfacial tension, γ_{SV} is the solid-vapor interfacial tension, and γ_{SL} is solid-liquid interfacial tension.

$$\gamma_{LV} cos\theta = \gamma_{SV} - \gamma_{SL} \quad (2)$$

This method of surface characterization is used widely in nanotechnological applications. For instance, Laure et al. used Diels-Alder chemistry to change the wettability of titanium oxide surfaces.[18] This switch in wettability was monitored with contact angle measurements. Brassard et al. used contact angle goniometry to study the effect of nanoparticle size on thin films containing fluorinated silica nanoparticles.[19] Their findings indicate that larger nanoparticle sizes resulted in larger contact angles.

1.2.2.3 Inductively Coupled Plasma Optical Emission Spectroscopy

Inductively coupled plasma optical emission spectroscopy (ICP-OES) is a powerful analytical technique used for the detection of trace metals. Figure 7 shows a schematic diagram of ICP-OES.

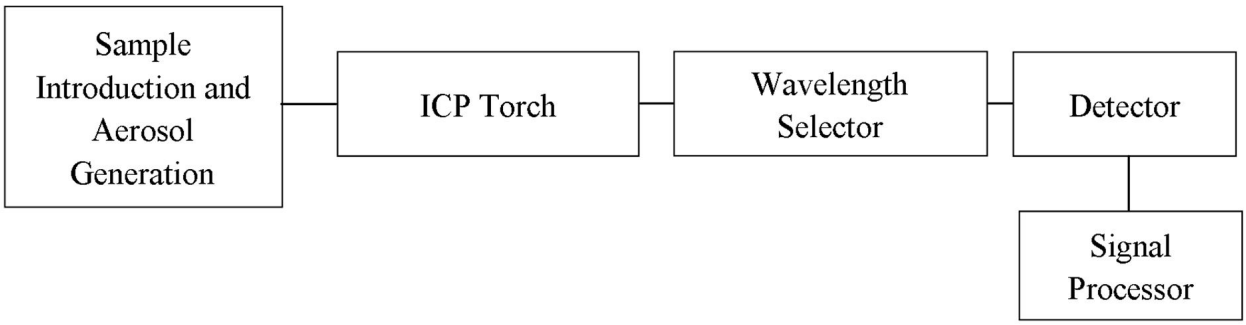

Figure 7. Schematic diagram of ICP-OES. Figure adapted from Baysal et al.[20]

Although this technique is often used in determining the elemental composition of soils, ICP-OES is also utilized in nanoscience. Kim et al. fabricated $CuInTe_2$ and $CuInTe_{2-x}Se_x$ ternary gradient quantum dots (QDs) for potential applications in solar cells. The elemental composition of these QDs was determined with ICP-OES.[21] In the study conducted by Justo et al. on cadmium for lead cation exchange and surface chemistry of PbS colloidal QDs, ICP-OES was employed to determine the lead to cadmium ratio.[22] This ratio was then used to quantify the shell thickness of PbS/CdS QDs.

1.3 Current Research

The goal of my research project is *to develop a better understanding of the fundamentals and the mechanisms behind Au NP thin film degradation on glass substrates in ultrapure water (nH_2O).* The long-term goal is to successfully fabricate thin films of Au NPs on glass substrates that exhibit temporal stability in various storage media.

The thin films of Au NPs on glass substrates fabricated in this research contain three main components. Using a layer-by-layer immersion method, shown in Figure 8, a layer of the coupling agent ((3-aminopropyl)trimethoxysilane or APTMS) is deposited onto the glass (SiO_2) microscope slide.

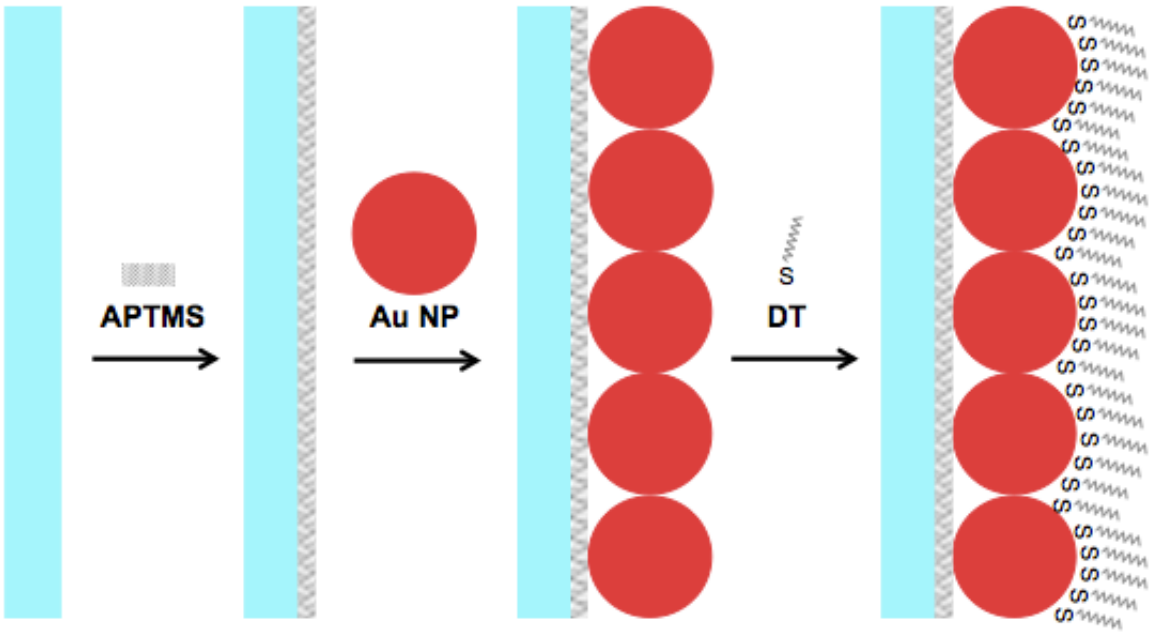

Figure 8. Schematic of Au NP-based thin film fabrication.

The next layer is composed of Au NPs, which bind strongly to the amine group of the coupling agent. Topping off the thin film is a layer of 1-dodecanethiol (DT) that binds to the layer of Au NPs with its reactive sulfur terminus. Upon the completion of thin film fabrication, thin films are immersed in a storage solution (nH_2O) to investigate its temporal stability over a period of seven days.

Previous research done by Alexandria Bear, illustrated in Figure 9, showed that Au NP thin films in storage solution (nH_2O) degrade over time.[23,24]

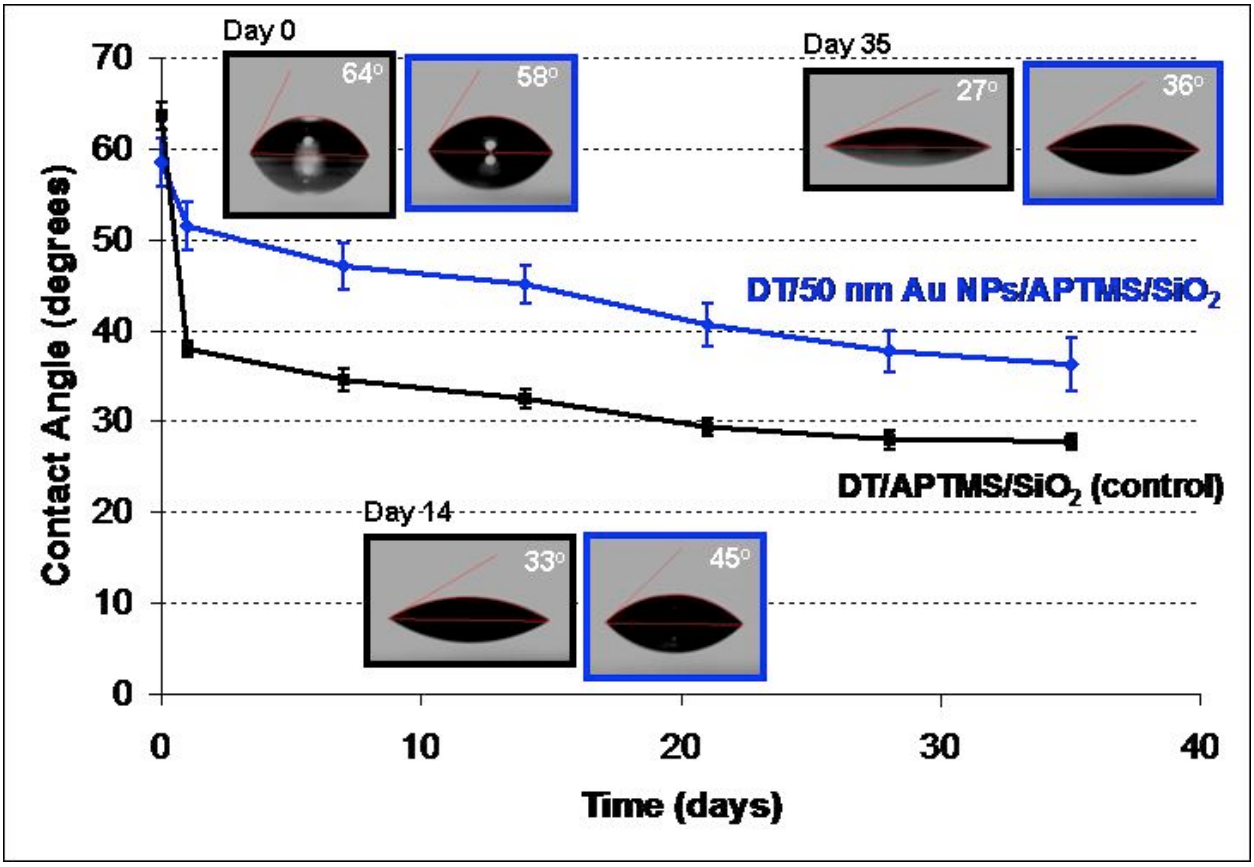

Figure 9. Temporal stability of commercially available 50 nm Au NP-based thin films. Surface wettability was assessed after 0, 1, 7, 14, 21, 28, and 35 days. Image modified from Bear's thesis.[23,24]

Because the final layer of these thin films is very hydrophobic, degradation of Au NP thin film is characterized by a decrease in contact angle over time. The most dramatic drop in contact angle was between the day 0 and the day 1 measurements. Over time, contact angles of the thin films reached a plateau.

Two possible mechanisms behind thin film degradation will be explored. First, thin film degradation might be because of the loss of Au NPs from the thin films.[25] If Au NPs desorb from the thin films, the DT molecules absorbed to those Au NPs are also lost from the thin film surface. This would result in a decrease in contact angle. ICP-OES will be employed to investigate whether the Au NP thin films exhibit a loss in Au NPs in storage solution (nH_2O). Another potential mechanism behind thin film degradation is the desorption of DT molecules

into the storage medium via oxidation of the thiolate headgroup. As illustrated by Flynn et al., loss of the alkanethiol layer integrity could be addressed with the introduction of an antioxidant into the storage solution.[26] Two antioxidants are studied: ascorbic acid and sodium ascorbate.

We employ several techniques to characterize and to monitor the temporal stability of the Au NP thin films. Contact angle goniometry is used to probe the wettability and uniformity of the monolayers. ICP-OES allows us to determine whether there is a loss of Au NPs after immersion into the storage medium. Ultraviolet-visible (UV-Vis) spectroscopy provides us information on the size and concentration of Au NPs. In addition to Au NP size, dynamic light scattering (DLS) also reports the uniformity of Au NPs in solution.

2. Materials and Methods

2.1 Materials

Potassium tetrachloroaurate (III) (99.995%) and sodium citrate tribasic dihydrate (ACS reagent ≥ 99.0%) were purchased from Sigma-Aldrich. Methoxypolyethylene glycol thiol (mPEG-SH, Laysan Bio, Inc.) was used as received. Chemicals (3-aminopropyl)trimethoxysilane (APTMS, Sigma-Aldrich) and 1-dodecanethiol (DT, Sigma-Aldrich) were diluted to 1% and 2 mM concentration with ethyl alcohol (EtOH, 200 proof, Pharmco/Koptec) respectively. Hydrochloric acid (HCl, ACS grade, BDH) and nitric acid (69-70%, ACS grade, BDH) were used as received. L-ascorbic acid (99+%, ACS reagent, Sigma-Aldrich) and L(+)-ascorbic acid sodium salt (> 99%, Fluka) for temporal stability studies were used as received. Glass microscope slides (SiO_2, 25 × 75 mm, 1.0 mm thick) were from VWR. Polypropylene centrifuge tubes of volumes 15 mL and 50 mL were obtained from Celltreat and Corning respectively. All water used for aqueous sample preparations and solutions was obtained from the Barnsted Nanopure Ultrapure Water System filtered to a resistivity of 18.2 MΩ × cm and hereafter will be referred to as nanopure water or nH_2O.

2.2 Gold Nanoparticle Synthesis

All glassware was cleaned with aqua regia (3:1 concentrated HCl:HNO_3). The glassware was then rinsed with nanopure water. Gold nanoparticles with a diameter of 11.2 nm were synthesized following the protocol by Flynn and Gerwith.[27] A 50 mL solution of 1.00 mM potassium tetrachloroaurate (III) was poured into a three-necked round bottom flask in a mineral oil bath at 100°C with constant stirring and allowed to equilibrate for 10 minutes. Then 5 mL of 38.8 mM sodium citrate tribasic dihydrate solution was added into the reaction flask and the reaction mixture was refluxed for 60 minutes at 100°C in the dark and wrapped with aluminum

foil. The reaction mixture was then removed from the oil bath and allowed to cool for 30 minutes with constant stirring. The synthesized gold nanoparticles were then transferred and stored in jars covered with aluminum foil.

2.3 Gold Nanoparticle Functionalization

To stabilize the gold nanoparticles, 2 mg of methoxypolyethylene glycol thiol (mPEG-SH) was dissolved for every 1 mL of gold nanoparticle solution. Methoxypolyethylene glycol thiol will hereafter be referred to as MPEG. A 5 mL aliquot of gold nanoparticle solution was PEGylated with 10 mg of MPEG, which was dissolved in 300 μL of nH_2O. The dissolved MPEG solution was slowly added to the gold nanoparticle solution with constant stirring. The solution was then stirred overnight.

2.4 Nanoparticle Characterization

Bare and PEGylated gold nanoparticles were characterized with both UV-visible spectroscopy and dynamic light scattering. Size and stability of the gold nanoparticles were determined through these measurements.

2.4.1 Ultraviolet-visible Spectroscopy

UV-vis spectra were collected with a Varian Cary 500 Scan UV-visible-NIR spectrophotometer. Shown in Table 1 are the settings used to obtain a UV-vis spectrum. Nanopure water was used to record a spectral baseline. Gold nanoparticle samples were diluted 1:10 in nanopure water with a total volume of 3 mL.

Table 1. Cary 500 UV-vis settings.

Parameter	Setting
Mode	Double beam
Recording range	300 – 700 nm
Average time	0.100 s
Resolution	1.00 nm
Scan rate	600.00 nm/min

Spectra obtained with the Cary 100 UV-vis spectrophotometer used the same settings used for the Cary 500 but over a recording range of 200 to 800 nm.

Spectra were also acquired with a single-beam VIS-NIR Vernier spectrophotometer from Ocean Optics, Inc. The spectrophotometer was calibrated with nanopure water and the following parameters shown in Table 2 were used. Samples were also diluted at a 1:10 ratio to a total of 3 mL.

Table 2. Settings for single-beam VIS-NIR Vernier spectrophotometer.

Parameter	Setting
Recording range	380 – 800 nm
Sample time	45 ms
Samples to average	50

2.4.2 Dynamic Light Scattering

Dynamic light scattering (DLS) spectra were collected with a Malvern Zetasizer Nano-ZS running Zetasizer Software 6.0.1. Aliquots of bare and PEGylated gold nanoparticle solutions were sonicated for 30 seconds with a Branson Sonifier 250 ultrasonic horn at a constant Duty Cycle and an Output Control of 1 to 2. Approximately 1 mL of the sonicated samples were measured with a BD 3 mL syringe and then filtered through a 25 mm syringe filter with a 0.45 μm cellulose acetate membrane (VWR International) into a four-sided plastic "fluorescence" cuvette. The standard operating procedure used for all samples was gold2.sop. Shown in Table 3 were the standard operating procedure parameters used.

Table 3. Standard operating procedure (gold2.sop) for measurements of hydrodynamic diameter and polydispersity using dynamic light scattering.

Dispersant:	Water
Dispersant Viscosity (cP):	0.8872
Dispersant Refractive Index:	1.330
Material:	Gold
Material Refractive Index:	1.650
Material Absorption:	0.20
Temperature:	25°C
Equilibration Time (s):	120

2.5 Fabrication of Thin Films of Gold Nanoparticles on Glass Substrates

2.5.1 Cleaning the SiO_2 Surface

Glass microscope slides (SiO2) were placed into Teflon wells and immersed in 5 mL of aqua regia overnight. Upon removal from aqua regia, the glass substrates were rinsed with nH_2O and EtOH alternately three times. Slides were then dried under a stream of N_2 gas.

2.5.2 Deposition of Coupling Agent

A 1% APTMS in EtOH solution was prepared in a 50 mL centrifuge tube. The solution was vortexed for 10 seconds prior to use. Clean SiO_2 slides were immersed in 45 mL of 1% APTMS in EtOH for a minimum of 24 hours. Upon removal from APTMS, slides were rinsed with nH_2O and ethanol alternately three times and then dried under a stream of N_2 gas.

2.5.3 Deposition of Gold Nanoparticles

Synthesized 11.2 nm Au NPs were transferred into a 50 mL centrifuge tube covered with aluminum foil. Silanized glass microscope slides were immersed in approximately 40–45 mL solution of Au NPs for a minimum of 24 hours. Upon removal from Au NP solutions, the slide was rinsed with nH2O and EtOH alternately three times and then dried under a stream of N_2 gas.

2.5.4 Deposition of Alkanethiol

A 2 mM DT solution in EtOH was prepared in a 50 mL centrifuge tube. Slides with a thin film of Au NPs were immersed into a 45 mL solution of 2 mM DT in EtOH for a minimum of 24 hours. APTMS-functionalized slides without a thin film of Au NPs served as a control and were also immersed into a 2 mM DT in EtOH solution for a minimum of 24 hours. Upon removal from DT, slides were dried in a VWR 1320 gravity convection oven at 55°C for 10 minutes. The temperature knob was set at 3 and the high limit knob was set at 4.2. Slides were then left to dry in a darkened hood overnight.

2.6 Temporal Stability of Gold Nanoparticle-Based Thin Films

2.6.1 Thin Films in Ultrapure Water

SiO_2 slides that have completed the fabrication process were immersed in 45 mL of nH_2O in a 50 mL centrifuge tube. If slides contained Au NPs, centrifuge tubes were covered with aluminum foil. Static contact angle measurements were taken at 0, 1, 3, 5, and 7 days. Before taking a measurement, slides were removed from the storage solution and dried under a stream of N_2 gas. After the contact angle was measured, slides were dried under a stream of N_2 gas prior to immersion into the same storage solution.

2.6.2 Thins Films in Ultrapure Water with Antioxidant

SiO_2 slides that have completed the fabrication process were immersed in 45 mL of nH_2O containing either 1 mM ascorbic acid or 1 mM sodium ascorbate in a 50 mL centrifuge tube. If slides contained Au NPs, centrifuge tubes were covered with aluminum foil. Static contact angle measurements were again taken at 0, 1, 3, 5, and 7 days. Before taking a measurement, slides were removed from the storage solution and dried under a stream of N_2 gas. The storage solution was then sealed with parafilm and purged with N_2 gas for 10-15 minutes in order to deoxygenate

the storage solution. After the contact angle measurement was taken, slides were dried under a stream of N_2 gas prior to immersion into the same storage solution. The tops of the centrifuge tubes were also sealed with parafilm.

2.7 Characterization of Thin Films

2.7.1 Contact Angle Goniometry

Contact angle measurements were obtained with a VCA Optima contact angle goniometer using the VCA Optima XE software. A water droplet was dispensed onto the surface of the thin films and the static contact angle was measured. The water droplet was of a specified volume of 0.25 μL until the water dispenser could no longer dispense water droplets of equal volume. Water droplets were then manually dispensed. The volume dispensed was based on approximately six to seven clicks of the dispensing knob. Eight water droplets were dispensed on to slide in the pattern shown in Figure 10.

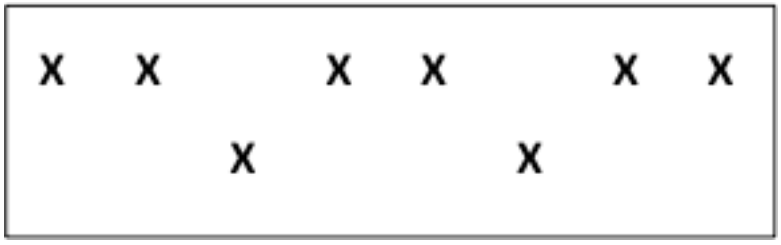

Figure 10. Pattern of water droplets for contact angle measurements.

After each step in the fabrication process, static contact angles of the thin films were measured. Each static contact angle reading gave two measurements. A total of 16 measurements are obtained with eight water droplets. The mean of the 16 measurements was calculated and Student t-tests were used to report data with a 95% confidence interval.

2.7.2 Inductively Coupled Plasma Atomic Emission Spectroscopy

Gold content of day 0 and day 7 slides were obtained with inductively coupled plasma atomic emission spectroscopy (PerkinElmer Optima 7000 DV ICP-AES). The wavelength at 267.595 nm for gold was selected. Au^{3+} standards (0.5 ppm, 2 ppm, 5 ppm, 10 ppm, and 30 ppm) were prepared with tetrachloroaurate (III) and high purity 2% nitric acid in 15 mL centrifuge tubes pretreated with 2% nitric acid.

To standardize the decrease in Au^{3+} concentration between day 0 and day 7 amongst samples, the percentage loss of Au^{3+} was calculated (Eq. 3).

$$\%\ of\ [Au^{3+}]\ loss = \frac{[Au^{3+}]_{Day\ 0} - [Au^{3+}]_{Day\ 7}}{[Au^{3+}]_{Day\ 0}} \times 100 \quad (3)$$

The mean percentage loss of Au^{3+} and standard deviation were determined.

2.7.2.1 Preparation of Samples for ICP-AES

Centrifuge tubes (50 mL) were treated with 2% nitric acid overnight. The 2% nitric acid wash was discarded and the pretreated centrifuge tubes were air-dried prior to use. Day 0 and 7 DT/Au NPs/APTMS/SiO_2 substrates were digested with 5 mL of aqua regia in a Teflon well for 10 minutes. The digest was then transferred into a dry 50 mL centrifuge tube that had been pretreated with 2% nitric acid. The Teflon well that contained the digestion was rinsed with 10 mL of nH_2O once and then transferred into the centrifuge tube. The volume of the digestion was then brought up to a total volume of 40 mL with nH_2O. Centrifuge tubes were covered with aluminum foil.

2.7.3 Optical Imaging

Pictures of slides with thin films of Au NPs were taken at the following stages of fabrication and stability studies: post-Au NPs, post-DT/Day 0, Day 1, Day 3, Day 5, and Day 7.

Slides were placed on a white sheet of paper and images were taken with a Samsung Galaxy S3 and Samsung Galaxy S5 camera at 2.0× zoom.

3. Results and Discussion

3.1 Synthesis and Characterization of Gold Nanoparticles

Gold nanoparticles were synthesized and characterized with dynamic light scattering and UV-vis spectroscopy. Dynamic light scattering was used to measure the size and the uniformity of the Au NPs suspended in solution. This method of characterization relates Brownian motion, the random movement of particles in a suspension, to particle size.[15] The size of the particle and the velocity of the Brownian motion are inversely related. Smaller particles will have a faster Brownian motion than larger particles. Because DLS infers the size of the particle based on how the particle diffuses within the suspension, the particle size measurement is referred to as the hydrodynamic diameter. Other factors that influence the hydrodynamic diameter are temperature, the viscosity of the fluid, surface structure of the particle, concentration, and the type of ions in the medium.

Gold nanoparticles formed by the reduction of $[AuCl_4]^-$ by sodium citrate tribasic are generally stable on their own and do not need ligand molecules to stabilize them because of an electric double layer that surrounds the synthesized Au NPs.[28] The first layer is comprised of citrate molecules that are adsorbed onto the surface of the Au NPs as well as any anions present in solution, such as chloride ions. Consequently, these species create a negatively charged surface. A positively charged layer surrounding the negatively charged layer is formed from cations, such as K^+, that are present in the reaction. By having this electric double layer, the resulting electrostatic repulsions should, in theory, prevent aggregation and coalescence. Despite the presence of the electric double layer, it is not uncommon for Au NPs to aggregate.

The synthesized Au NPs were expected to have a hydrodynamic diameter of 11.2 nm. However, the hydrodynamic diameter of bare Au NPs were often found to be slightly larger than

11.2 nm. Table 4 shows the DLS results for bare and MPEG-functionalized Au NPs. Although DLS characterization of bare Au NPs often found the hydrodynamic diameter to be larger than 11.2 nm, by functionalizing Au NPs with MPEG, a good estimate of the size of the synthesized Au NPs could be determined.

Table 4. Characterization of a representative batch of bare and PEGylated Au NPs with DLS. The mean PDI and peak 1 were calculated from N=3 measurements.

Sample	Mean PDI	Mean Hydrodynamic Diameter (nm)
Bare Au NPs	0.12	16.8
MPEG/Au NPs	0.18	37.4

To prevent potential aggregation and coalescence of Au NPs while taking DLS measurements, an organic polymer, MPEG, was used to displace the anions at the surface of the Au NP and stabilize the particle. The chemical structure of MPEG is illustrated in Figure 11.

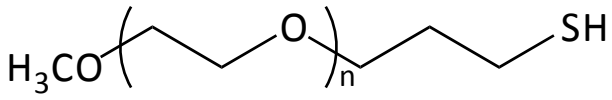

Figure 11. Chemical structure of methoxypolyethylene glycol thiol, where n indicates the number of ethylene glycol units.

This stabilizing ligand interacts with the Au NPs via thiol chemistry. MPEG is able to form a protective shell around the Au NPs by displacing the anions absorbed to the surface of Au NPs, thereby preventing the agglomeration of Au NPs. The expected thickness of the PEG layer around the particle is approximately 12 nm.[29,30] The hydrodynamic diameter of MPEG-functionalized Au NPs is approximately 35 nm. Therefore, if the mean hydrodynamic diameter of a representative batch of MPEG-functionalized Au NPs was approximately 37.4 nm, then the synthesized Au NPs were estimated to be about 13.4 nm in diameter.

Dynamic light scattering also provided quantitative information on the uniformity of the synthesized Au NPs. The polydispersion index (PDI) is a measure of homogeneity or the

heterogeneity of the particle population. PDI values can range from 0.00 (a monodisperse particle population) to 1.00 (a polydisperse population). For the thin film studies, only synthesized Au NPs with a PDI of 0.3 or less were used.

UV-vis spectroscopy is a valuable technique for probing Au NPs because the particles possess a sensitive surface plasmon band.[28] Citrate-stabilized Au NP solutions exhibited a characteristic red color. Gold nanoparticles functionalized with MPEG also produced a red solution. UV-vis spectroscopy was used to characterize the optical profile of the synthesized Au NPs and the functionalized Au NPs. Figure 12 shows the optical signature of bare Au NPs. An absorbance peak at approximately 519 nm was observed. A 1–2 nm peak variation was occasionally observed from sample to sample. When the Au NPs were functionalized with MPEG, a redshift of approximately 1–3 nm was typically observed. The redshift to a longer wavelength was likely a consequence of an increase in interparticle distance when Au NPs were functionalized with MPEG, which in turn altered the surface plasmon resonance properties of the Au NPs.[31] Changes in surface plasmon resonances are associated with particle size and the surrounding medium.[28] UV-vis spectroscopy can monitor these changes in the optical properties of Au NPs.

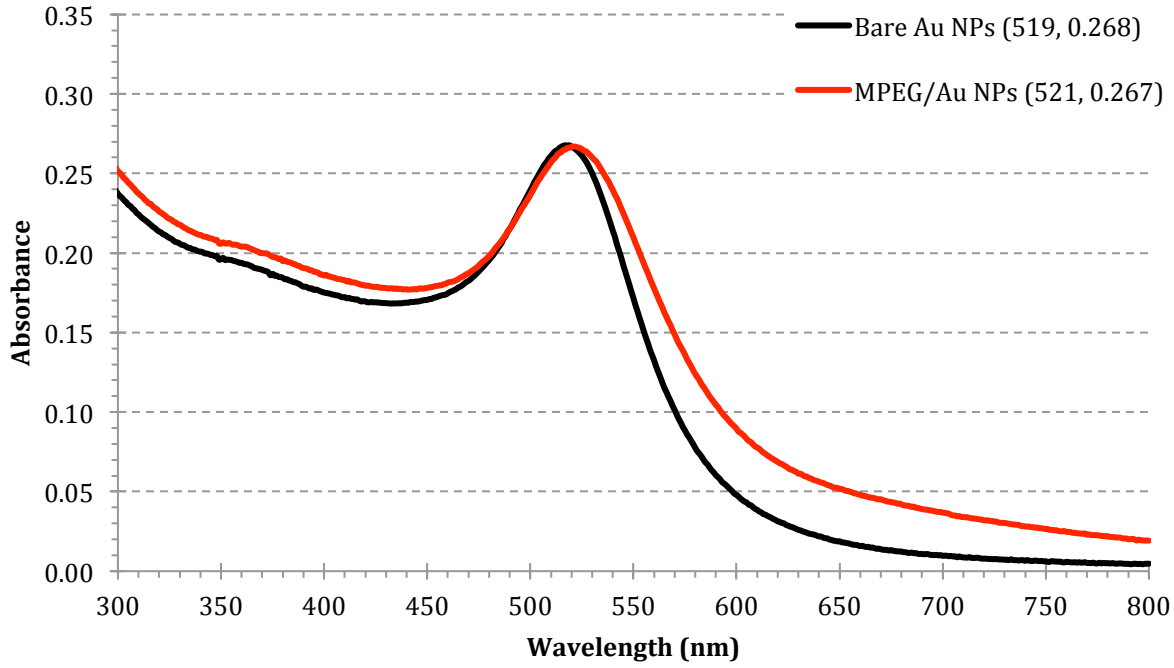

Figure 12. UV-vis spectra of bare and PEGylated Au NPs.

3.2 Fabrication of Thin Films of Au NPs on Glass

Thin films of Au NPs on silicon dioxide (SiO_2) glass microscope slides were fabricated with a layer-by-layer immersion technique. Contact angle goniometry was used to characterize the thin films at every step of the thin film fabrication process.[12] The water droplet that was dispensed onto the substrate behaved in a manner unique to the particular layer on the surface of the glass substrate. Therefore, this characterization technique can be used to confirm the presence of a newly added layer on the glass substrates. In addition, the uniformity of these thin films can be assessed.

Table 5 and Figure 13 present the mean static contact angles and representative images of static contact angles of the thin films at each step of the thin film fabrication process, respectively. Previous work reported similar values for each step of the fabrication process, with

the exception of the deposition of DT.[23,24] The following sections describe the changes in contact angle that occurred during the film formation process.

Table 5. Mean static contact angle of thin films during fabrication process. Data are reported as CA ± 95% CI.

Sample	Mean Contact Angle (°)
SiO_2 (initial)*	6.4 ± 0.3
SiO_2 (cleaned w/ Aqua Regia)*	13.6 ± 0.4
APTMS/SiO_2*	48.1 ± 0.3
Au NPs/APTMS/SiO_2^	24.2 ± 0.5
DT/APTMS/SiO_2^	69.6 ± 0.6
DT/Au NPs/APTMS/SiO_2^	83 ± 1

*Mean CA was calculated from N=384 CA measurements.
^Mean CA was calculated from N=192 CA measurements.

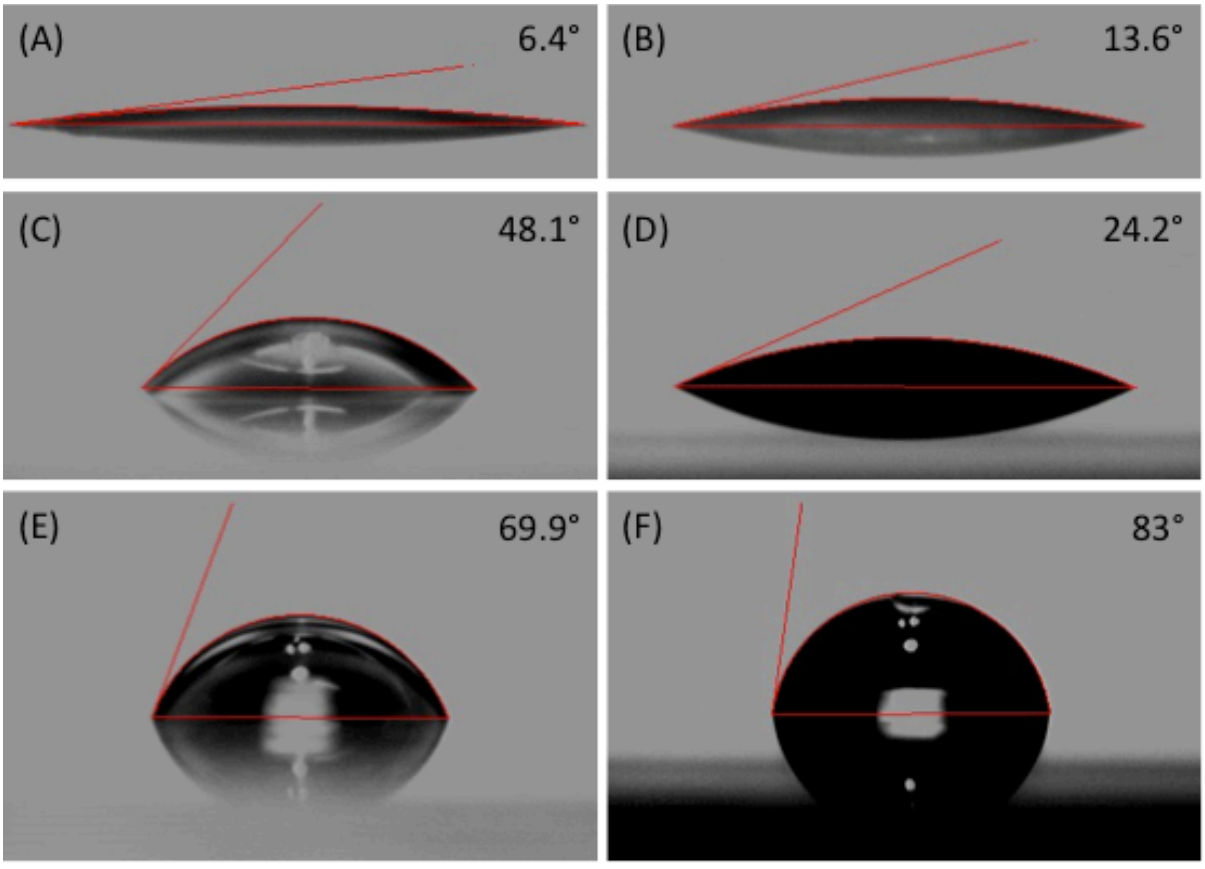

Figure 13. Representative images of static contact angles of thin films during fabrication process: (A) Initial SiO_2, (B) cleaned SiO_2, (C) APTMS/SiO_2, (D) Au NPs/APTMS/SiO_2, (E) DT/APTMS/SiO_2 (control), and (F) DT/Au NPs/APTMS/SiO_2.

3.2.1 Preparation of SiO_2

Slides prior to treatment with aqua regia had mean contact angles of 6.4 ± 0.3°, which indicated that the surface of the substrates is very hydrophilic. In order to oxidize any contaminants on the surface of the glass substrate, the slides were immersed in aqua regia overnight. Once the glass substrates were removed from the aqua regia, they exhibited mean contact angles of 13.6 ± 0.4°. Bear reported similar values for this step of the fabrication process despite the use of a different cleaning agent.[23] Clean slides prepared with piranha solution (1:3 v/v 20% H_2O_2 and concentrated H_2SO_4 mixture) had static contact angles of approximately 15°. In addition to removing contaminants from the surface, the aqua regia treatment on the glass substrates created a fully protonated surface on the substrate, which was a key component to the addition of the next layer.

3.2.2 Addition of Coupling Agent

The coupling agent, APTMS, was bound to the silanized-SiO_2 surface through a condensation reaction as depicted in Figure 14.

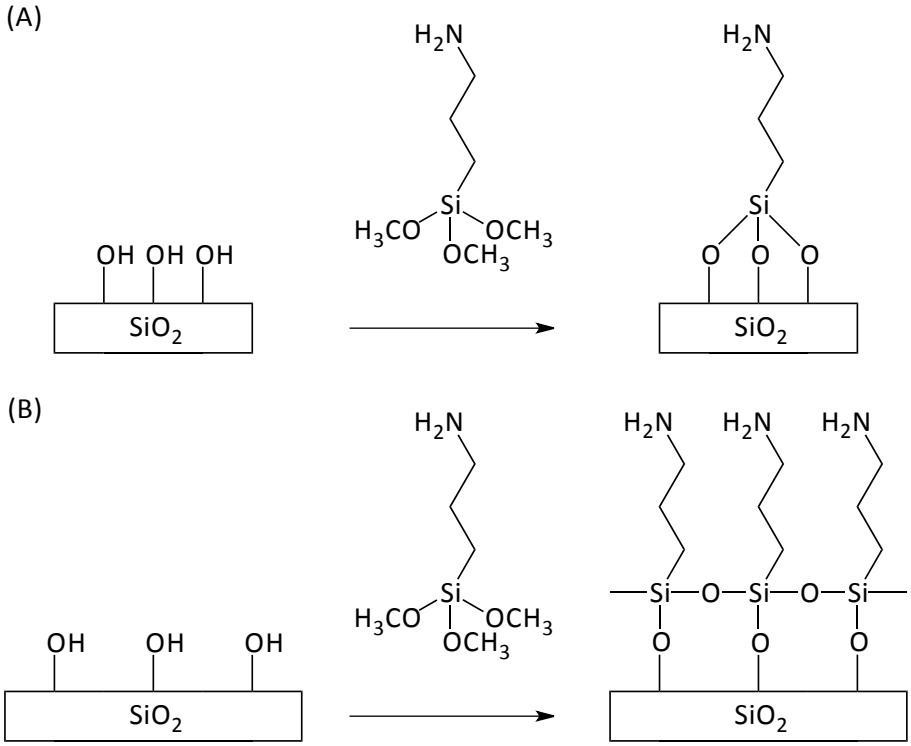

Figure 14. Condensation reaction between silanol surface of silicon dioxide glass microscope slide and coupling agent, 3-aminopropyltrimethoxysilane (APTMS): (A) schematic 1 and (B) schematic 2.

Glass substrates functionalized with APTMS had an increased average static contact angle of approximately 35°, indicating a more hydrophobic interaction between the surface of the substrate and the water droplet. After at least 24 hours of exposure to APTMS in EtOH, a mean contact angle of 48.1 ± 0.3° was observed for APTMS-functionalized slides. Despite the presence of terminal amines and hydroxyl groups that have hydrogen bonding capabilities, the nonpolar hydrocarbon chain of APTMS molecules appeared to contribute more to the decrease in surface wettability. Although a different deposition technique was used, Song et al. found that silicon dioxide substrates functionalized with APTMS had a contact angle of approximately 54.5°.[32] On the other hand, Bear and Lin reported slightly lower contact angles for APTMS-modified substrates (approximately 40° and 30 ± 2°, respectively).[23,24] APTMS-functionalized

substrates appear to have a wide range of surface wettability, which can be attributed to a variety of factors such as deposition technique and exposure time to APTMS.[32,33]

3.2.3 Functionalization of APTMS/SiO_2 with Au NPs

A decrease in mean static contact angle of approximately 24° was observed when Au NPs were deposited onto APTMS/SiO_2 substrates (mean CA = 24.2 ± 0.5°). Similarly, Bear reported contact angles of approximately 25° after the deposition of 11.2 nm Au NPs onto APTMS-functionalized substrates.[23] The increase in wettability can be attributed to the high radii of curvature of nanoparticles, which introduces surface roughness to the thin films. Nanoparticle size and radius of curvature are inversely related.[12] As nanoparticle size decreases, the radius of curvature increases, which in turn increases surface roughness. Consequently, a decrease in contact angle is expected because the surface of the substrate may have defects and is not planar. The surface roughness brought about by Au NPs will also affect the deposition of DT molecules.

Substrates functionalized with Au NPs varied in color as shown in the optical images of slides in Figure 15. The changes in color are a consequence of aggregation. When the interparticle distance decreases, the surface plasmon resonance of Au NPs changes and a blue color is observed.[34]

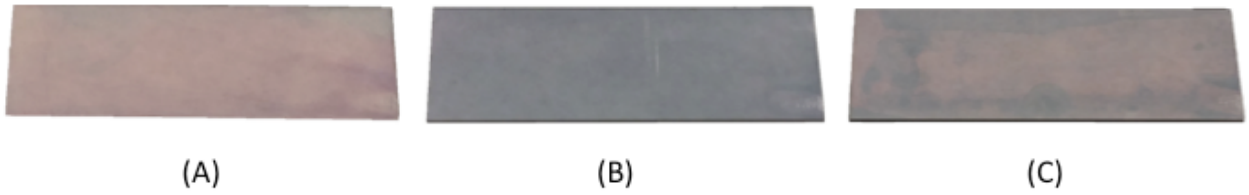

Figure 15. Representative images of slides functionalized with Au NPs. Colors range from (A) pink to (B) blue or (C) some combination of both. Images were taken with a Samsung Galaxy S5 at 2.0× zoom on a white surface.

3.2.4 Deposition of DT on Thin Films

Thin films without Au NPs were fabricated to serve as controls so that comparisons between thin films containing Au NPs and thin films without Au NPs can be made. APTMS-

modified substrates were immersed in a DT in EtOH solution for 24 hours and then dried in an oven at 55 °C for 10 minutes. Temperature drops of 1–5 °C were typical after the oven had been opened and then closed. A mean static contact angle of 69.6 ± 0.6° was observed for DT/APTMS/SiO_2 substrates. The hydrophobic character of these slides can be attributed to the aliphatic hydrocarbon tails of the DT molecules.

Surface wettability measurements for DT-coated Au NP thin films increased significantly in comparison to slides with just Au NPs. The mean static contact angle was 83 ± 1°. In contrast Bear reported a contact angle of less than 20° while the contact angles of DT/Au NPs/APTMS/SiO_2 substrates reported here were much higher.[23] DT molecules readily self-assemble onto gold nanoparticles. The thiol headgroups of the DT molecules interact with the Au NPs forming a covalent bond. Additionally, the van der Waals interactions between the aliphatic hydrocarbon tails allow the DT molecules to form a thin film on top of the Au NPs. As a result, this final layer has a very hydrophobic character so a high contact angle was expected.

Slides absent of Au NPs remained clear and transparent throughout the fabrication process. After the deposition of DT molecules onto Au NP-containing substrates, a change in color was observed. Slides that were initially pink often turned blue. Occasionally, the coloration of DT/Au NPs/APTMS/SiO_2 substrates was a mix of both pink and blue. Au NP-modified slides that were blue in color often gained a more intense blue coloration after immersion in DT solution. The color changes seen in this fabrication step can be attributed to the changes in the surface plasmon resonance of Au NPs as interparticle distance decreases.[34]

3.3 Temporal Stability of Gold Nanoparticle-based Thin Films

The stability of the gold nanoparticle-based thin films was investigated over seven days. Shown in Figure 16 is the time-dependent behavior of controls (DT/APTMS/SiO_2) and Au NP-

containing samples (DT/Au NPs/APTMS/SiO_2). Surface wettability was assessed after 0, 1, 3, 5, and 7 days. In the temporal stability studies with storage in nH_2O, a significant difference in static contact angle was observed between controls and Au NP-containing slides.

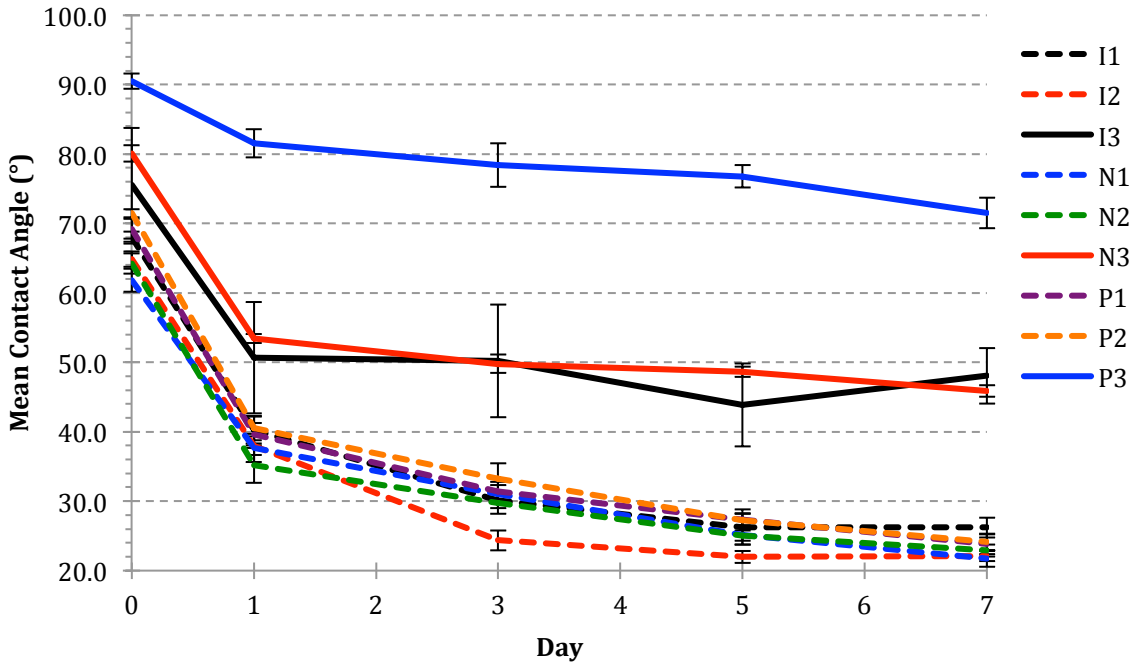

Figure 16. Temporal stability of DT/APTMS/SiO_2 (control, dashed lines) and DT/Au NPs/APTMS/SiO_2 (solid lines) thin films in nanopure water for seven days. Surface wettability was assessed after 0, 1, 3, 5, and 7 days. Data are reported as CA ± 95% CI, where the mean CA was calculated from N=16 CA measurements.

The final layer in the fabrication process was composed of a very hydrophobic molecule (DT). Therefore, both control and sample slides started out with a high initial contact angle, which ranged from 62° to 72° and 80° to 91°, respectively. Upon immersion in storage solution (nH_2O), a marked decrease in static contact angle was observed for both controls and samples. The greatest decrease in contact angle occurred between day 0 and day 1. The magnitude of the change was similar between controls and samples, averaging approximately 27°, with the exception of one sample (P3, solid blue line). From day 1 to day 7, both DT/APTMS/SiO_2 and DT/Au NPs/APTMS/SiO_2 slides exhibited a steady decrease in contact angle.

Even though the thin films were fabricated under similar conditions, the static contact angle varied from sample to sample. However, the static contact angles among Au NP-containing samples exhibited much more variability, as indicated by the larger confidence intervals, than the controls. Although varied, controls still showed some degree of overlap suggesting that the temporal stability data was reproducible for slides without Au NPs. The same cannot be said for the Au NP-containing slides. Two Au NP-containing samples (I3 and N3), represented by the black and red solid lines, respectively, had overlapping contact angles to some degree. However, the contact angles of the third sample (P3), represented by the blue solid line, did not overlap with the contact angles of the other two samples. Despite the overlap between samples I3 and N3, Au NP-containing slides generally had larger 95% confidence intervals in comparison to the controls, suggesting a lack of surface uniformity even across a single Au NP-containing slide.

3.4 Investigating the Mechanisms of Degradation of Thin Films

From the temporal stability studies of thin films in nH_2O, the largest drop in contact angle occurred between when the thin films have completed the fabrication process (Day 0) and after immersion in nH_2O for 24 hours (Day 1). The top-most layer of the thin films was composed of DT, a very hydrophobic molecule. Therefore, a high initial contact angle (Day 0) was observed and any decrease in contact angle could be attributed to the loss of DT molecules from the thin films. Two possible mechanisms of degradation were explored: (1) the desorption of DT molecules from the thin films by oxidation and (2) the desorption of Au NPs from the thin films.

3.4.1 Desorption of DT from Thin Films

Flynn et al. investigated the long-term stability of self-assembled alkanethiol monolayers on gold surfaces in biological media.[26] SAM loss was observed over time and potential

mechanisms of SAM desorption were investigated. One proposed desorption mechanism was the oxidation of the thiolate headgroup to sulfinates and sulfinites followed by desorption into the surrounding medium. To counter this SAM desorption mechanism, a small concentration of uric acid, an antioxidant, was added into the storage solution. Various surface characterization techniques determined that no monolayer loss occurred. Therefore, a possible degradation mechanism for this system of gold nanoparticle-based thin films is the desorption of DT molecules by oxidation. To address the oxidation of the DT molecules, a small concentration (1 mM) of antioxidant (ascorbic acid or sodium ascorbate) was added into the nH_2O storage solution. In addition, the nH_2O with antioxidant storage solution was deoxygenated by bubbling N_2 gas into the storage solution for 10 to 15 minutes every time the thin films were taken out for contact angle measurements.

Changes in the integrity of Au NP-containing thin films were investigated over seven days in nH_2O with 1 mM of an antioxidant. Illustrated in Figure 17 is the temporal stability of controls (DT/APTMS/SiO_2) and Au NP-containing samples (DT/Au NPs/APTMS/SiO_2) in storage solutions containing either 1 mM ascorbic acid (A) or 1 mM sodium ascorbate (B). Similar to the temporal stability studies conducted in just nH_2O, a statistical difference was observed between controls and samples in both storage solution conditions. Over the seven-day period, Au NP-based thin films retained higher contact angles than the controls.

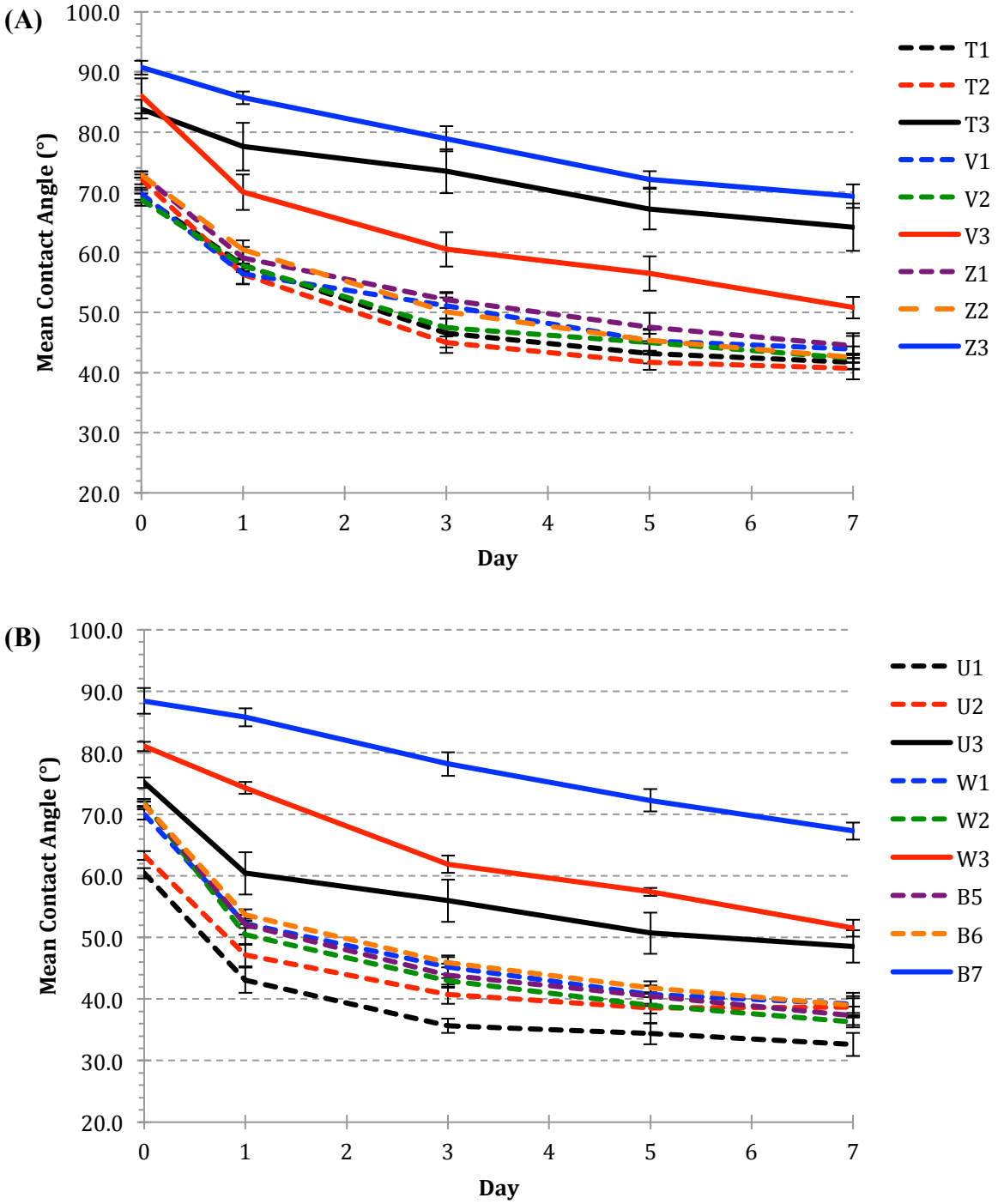

Figure 17. Temporal stability of thin films in nanopure water with **(A)** 1 mM ascorbic acid and **(B)** 1 mM sodium ascorbate. Solid lines are for Au NP-containing samples and dashed lines for controls absent Au NPs. Surface wettability was assessed after 0, 1, 3, 5, and 7 days. Data are reported as CA ± 95% CI, where the mean CA was calculated from N=16 CA measurements.

The addition of antioxidant in the storage solution (nH_2O) improved thin film quality. Initial (Day 0) contact angles of controls and samples ranged from 68° to 73° and 84° to 91°, respectively. The contact angles of these thin films are within the same range as the thin films used in the temporal stability studies with just nH_2O (Section 3.3) but with a smaller range. In addition, the greatest decrease in contact angle still occurred between day 0 and day 1. However, in comparison to thin films in nH_2O without antioxidant, the thin films immersed in storage solution containing 1 mM ascorbic acid had a smaller decrease in contact angle from day 0 to day 1. A mean difference of 13° and 9° was observed for controls and samples respectively. By comparison, when immersed in just nH_2O, the mean magnitude of change of both control and sample slides was 27°. With the addition of ascorbic acid in the storage solution, the decrease in the magnitude of change between day 0 and day 1 indicated that there might have been a decrease in the loss of DT by oxidation of the sulfhydryl followed by desorption into the surrounding environment.

Although the presence of an antioxidant resulted in better thin films initially (better retention of the hydrophobic character), the addition of an antioxidant appeared to change the time-dependent behavior of the thin films. For both controls and samples, although more noticeable in Au NP-containing samples, a steady drop in contact angle over the seven-day period was observed rather than a drastic decrease in contact angle between days 0 and 1 followed by eventual stabilization.

Similar results were obtained with sodium ascorbate as the antioxidant. The controls and Au NP-containing samples had initial contact angles (Day 0) that ranged from 60° to 72° and 75° to 88°, respectively. Among the controls the largest drop in hydrophobicity, averaging at approximately 18°, was observed from day 0 to day 1. In contrast, the greatest decrease in

contact angles among the Au NP-based thin films varied between day 0 to day 1 (U3) and day 1 to day 3 (W3 and B7). Instead of experiencing a drastic drop in contact angle within the first 24 hours of immersion in storage solution, contact angles of Au NP-based thin films appeared to decrease more steadily over the seven-day period. Controls experienced a similar moderate drop in contact angle over time. The lack of overlap in contact angle in the Au NP-containing samples suggested that there was not a high degree of reproducibility among Au NP thin films stored in nH_2O with antioxidant. For both controls and Au NP thin films, no stabilization by the end of the seven-day period was observed.

The time-dependent behavior of controls and Au NP-based thin films in different storage solutions are compared against each other in Figure 18 and Table 6. The integrity of controls and sample slides were better retained when stored in nH_2O with antioxidant. This was especially the case for controls and Au NP-based thin films immersed in nH_2O with sodium ascorbate (blue lines) in comparison to their counterparts immersed in only nH_2O (black lines). The control samples and the Au NP-containing samples in both storage solutions started at approximately the same initial contact angle. From day 0 to day 1, the drop in contact angle was much smaller in the controls and samples immersed in nH_2O with 1 mM sodium ascorbate (18.4° and 7.2°, respectively) than the controls and samples stored in just nH_2O (28.1° and 18.5°, respectively). For the nH_2O with 1 mM ascorbic acid condition (red lines), controls and samples had a higher initial (Day 0) contact angle and retained that higher contact angle throughout the seven-day period with respect to the other two storage conditions. This higher starting contact angle may be attributed to various external factors including, but are not limited to, temperature, humidity, size of synthesized Au NPs, and exposure to air.[35]

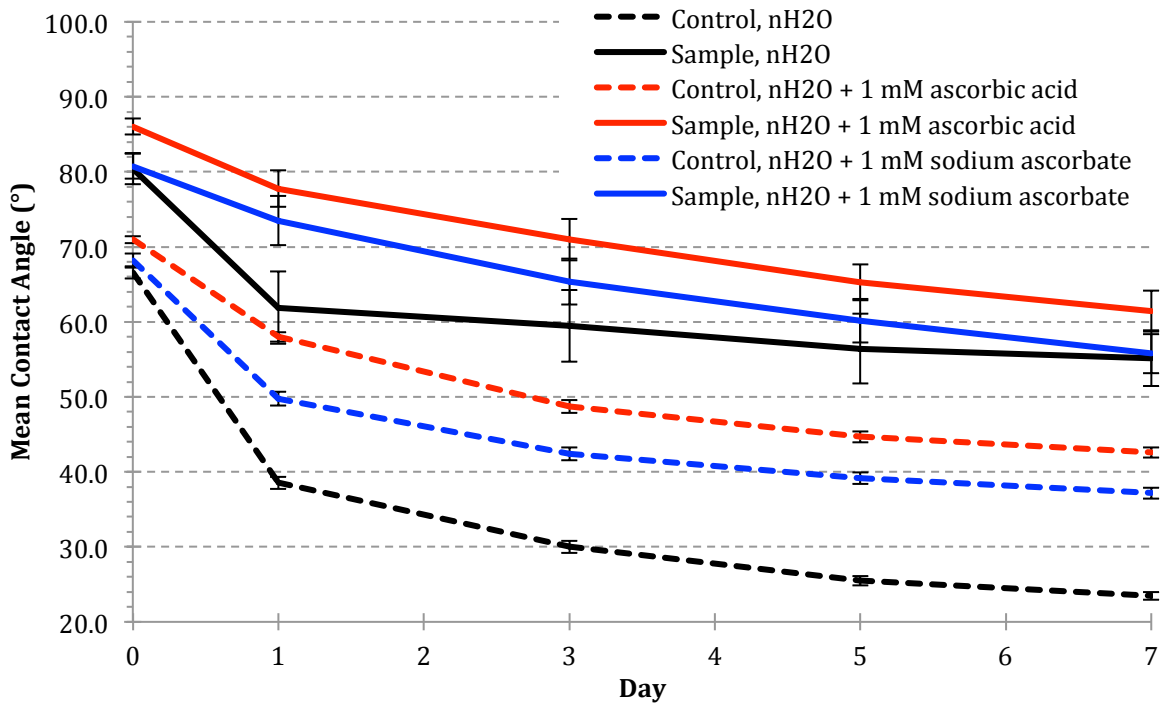

Figure 18. Comparison of temporal stability studies of DT/APTMS/SiO_2 (control, dashed lines) and DT/Au NPs/APTMS/SiO_2 (sample, solid lines) thin films in nanopure water w/ 1 mM of antioxidant. Surface wettability was assessed after 0, 1, 3, 5, and 7 days. Data are reported as CA ± 95% CI, where the mean CA was calculated from N=96 CA measurements for control slides and N=48 for sample slides.

Table 6. Contact angle measurements for thin films in storage solutions with no antioxidant, ascorbic acid, and sodium ascorbate at critical points: days 0, 1, and 7. Samples contained Au NPs while controls did not have any Au NPs. Data are reported as mean CA ± 95% CI, where the mean CA was calculated from N=96 CA measurements for control slides and N=48 for sample slides.

Storage Solution	**Type**	**Mean Contact Angle (°)**		
		Day 0	*Day 1*	*Day 7*
nH_2O	Control	66.6 ± 0.8	38.5 ± 0.8	23.5 ± 0.5
	Sample	80 ± 2	62 ± 5	55 ± 4
1 mM ascorbic acid in nH_2O	Control	71.0 ± 0.5	58.0 ± 0.6	42.6 ± 0.7
	Sample	86 ± 1	78 ± 2	61 ± 3
1 mM sodium ascorbate in nH_2O	Control	68 ± 1	50 ± 1	37 ± 1
	Sample	81 ± 2	73 ± 3	56 ± 3

By the end of the seven-day period, controls in storage solutions with antioxidant retained a higher contact angle than the controls in nH_2O. However, Au NP-containing samples stored with sodium ascorbate (solid blue line) converged at the same point, approximately 55°, that

samples in nH_2O (solid black line) leveled off at after seven days. Despite having a higher contact angle overall, the Au NP-based thin films stored in nH_2O with ascorbic acid (solid red line) behaved similarly to the respective substrates stored in nH_2O with sodium ascorbate. If the Au NP-based thin films stored with ascorbic acid had started at an initial contact angle (Day 0) that was shifted down by approximately 10°, then those substrates probably would have leveled off at the same point as both the samples in nH_2O and nH_2O with sodium ascorbate. Under all three storage conditions, the difference in contact angle between day 0 and day 7 among the Au NP-containing thin films was approximately 25°. In contrast, the magnitude of change between day 0 and 7 for the controls in ascorbic acid and sodium ascorbate were 28° and 31°, respectively, whereas the controls in nH_2O exhibited a difference of 43°.

Au NP-based thin films in all three storage conditions experienced high variability as illustrated by the large confidence intervals while the controls for each of the three storage conditions showed little variability. This can be attributed to a small sample size of Au NP-based thin films. Other factors that could contribute to the variability include, but are not limited to, heating temperature, the synthesized Au NPs, and handling of the slides. Studies have shown that heating time and heating temperature can affect the morphology and the optical properties of thiol encapsulated gold nanoparticle thin films.[7,36] In addition, the coupling agent (APTMS) may not be behaving as expected. Some potential interactions of APTMS with the SiO substrate are illustrated in Figure 19.[33]

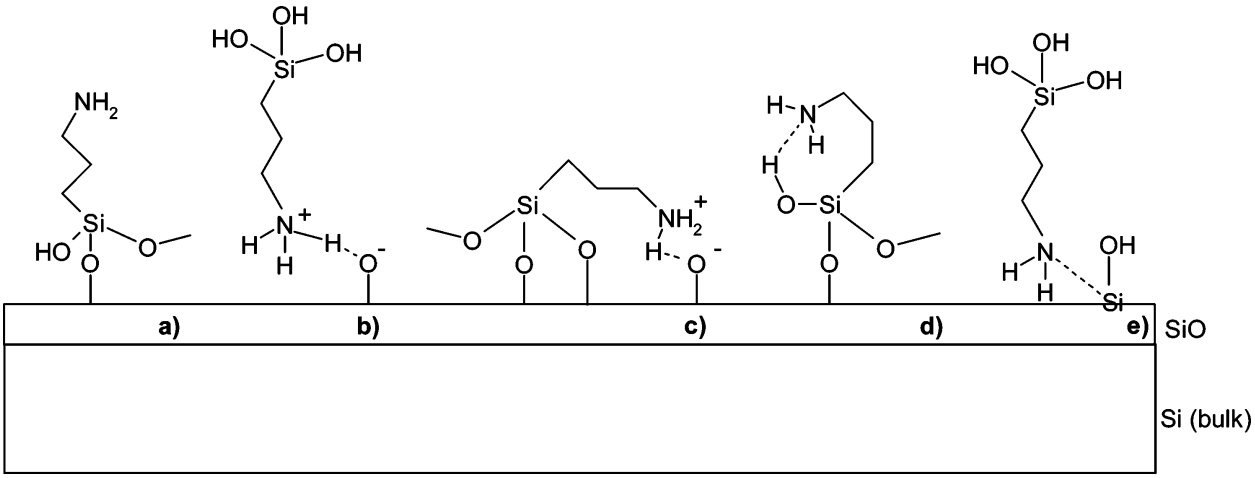

Figure 19. Different adsorption mechanisms of (3-aminopropyl)-triethoxysilane (APS) and APTMS on SiO proposed in the literature.[37] Figure taken from Kristensen et al.[33]

If APTMS adsorbed similarly to mechanisms (c) or (d), there may be dents or defects when Au NPs are deposited onto an APTMS-functionalized substrate. This would further impact the self-assembly of DT molecules on Au NPs, which could result in more exposure to oxidation. Therefore, some samples may have deviated from their expected behavior because of exposure to different variables and external factors.

3.4.2 Desorption of Gold Nanoparticles from Thin Films

Shown in Figure 20 are representative images of DT/Au NPs/APTMS/SiO_2 substrates starting from the deposition of Au NPs and through the temporal stability studies. Upon the addition of Au NPs onto the APTMS-functionalized substrate, a light pink color was observed. When the thin films were exposed to the air and the washing solutions (nH_2O and EtOH), an occasional change in color from pink to blue was observed. After the Au NP-modified substrates were immersed in DT, the thin films generally exhibited a blue coloration. Different storage solutions did not appear to affect the intensity of the coloration of the thin films over time because there were no noticeable differences. Although optical imaging of the Au NP-based thin

films provided qualitative information about the thin films, it could not provide any quantitative information about the loss of Au NPs from the surface of the thin films.

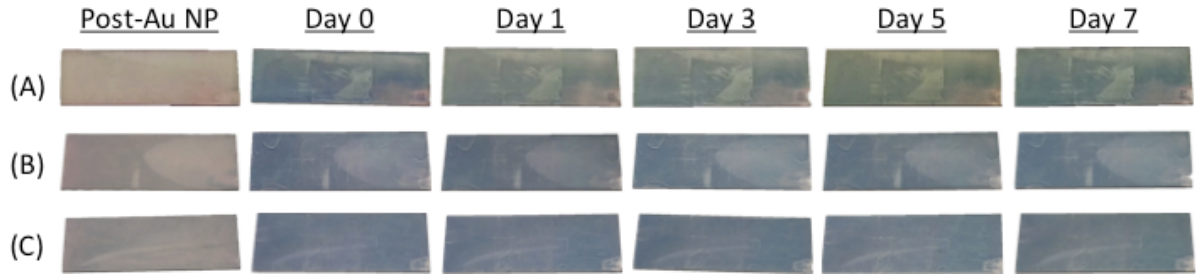

Figure 20. Representative images of DT/Au NPs/APTMS/SiO_2 during the fabrication process and throughout the seven-day immersion in (A) nH_2O, (B) nH_2O with 1 mM ascorbic acid, and (C) nH_2O with sodium ascorbate. Green coloration on some of the images in row (A) was a result of the angle at which the image was taken. No green coloration was observed. Images were taken with a Samsung Galaxy S3 (A) and a Samsung Galaxy S5 (B and C) at 2.0× zoom on a white surface.

To investigate whether the degradation of thin films was attributed to the loss of Au NPs from the thin films, trace metal analysis for Au^{3+} was performed with ICP-AES on day 0 and day 7 slides containing Au NPs. In order to determine the Au^{3+} concentration of the samples, a calibration curve was constructed from Au^{3+} standards of the following concentrations: 0.5 ppm, 2 ppm, 5 ppm, 10 ppm, and 30 ppm. Shown in Figure 21 is a standard calibration curve for [Au^{3+}] at 267.595 nm. The optimal calibration curve should exhibit high correlation among the data points, which is indicated by a linear regression value, R^2, close to or equal to one.

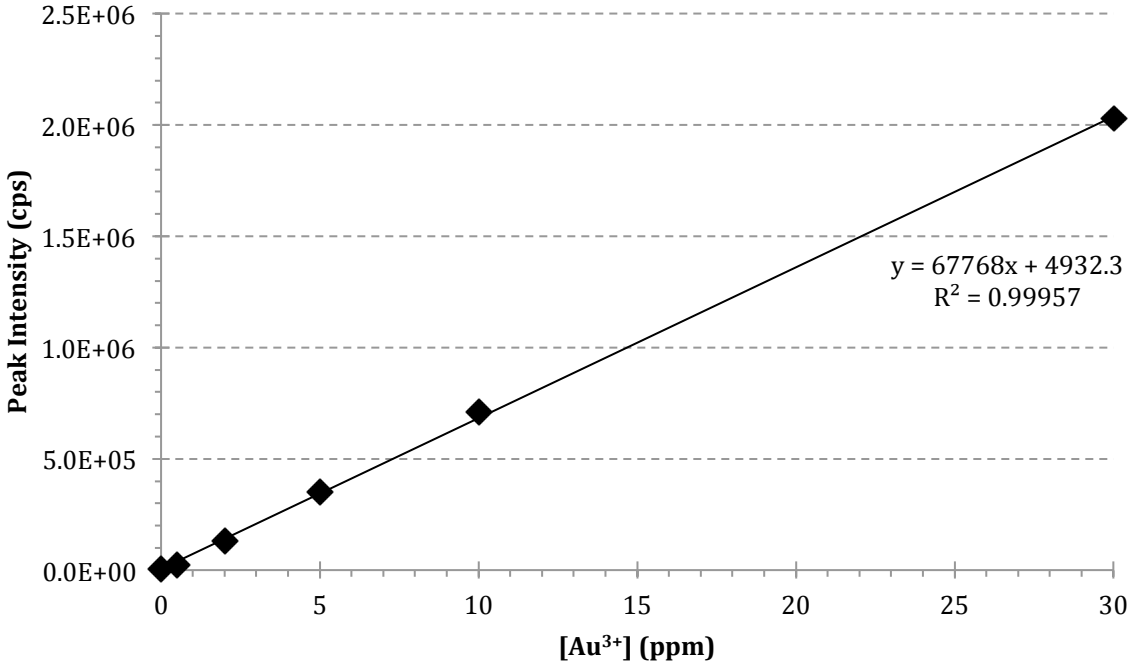

Figure 21. Standard calibration curve for [Au^{3+}] at 267.595 nm. [Au^{3+}] standards of 0.5, 2, 5, 10, and 30 ppm were prepared in aqua regia (3:1 HCl to HNO_3).

In preparation for ICP-AES analysis, day 0 and day 7 Au NP-containing samples were digested with aqua regia. Once a sample slide was digested, no further measurements could be made. Therefore, day 0 and day 7 slides were not the same slide. But during the fabrication process, they were immersed in the same solutions at the same time so they are considered a set. In a typical ICP-AES spectrum, as depicted in Figure 22, a difference in peak intensity at 267.595 nm, represented as Δ, was seen between day 0 and day 7.

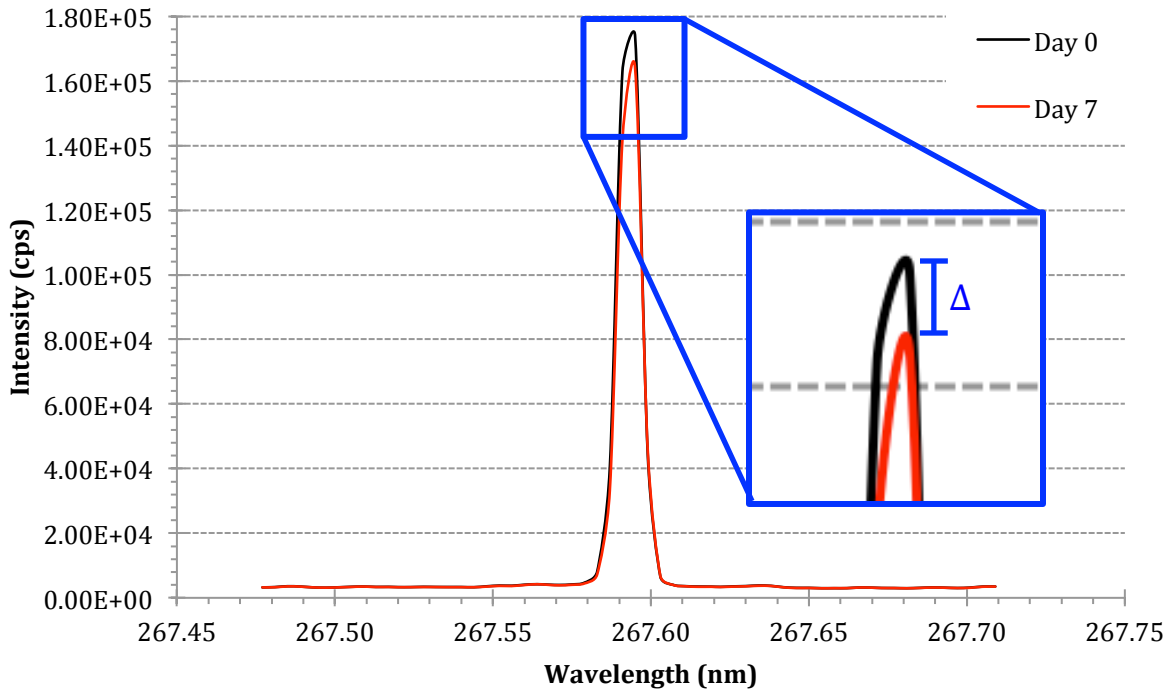

Figure 22. Representative ICP-AES spectrum of [Au^{3+}] of day 0 and 7 Au NP-containing slides. Emission wavelength of 267.595 nm was used to detect Au^{3+}. Au NP-containing slides were digested with aqua regia.

Although a general decrease in Au^{3+} concentration was observed from day 0 to day 7 slides, the Au^{3+} concentration varied among samples prepared under similar conditions. Visually, some Au NP-based thin films were lighter than others. These lighter colored thin films often resulted in slightly lower Au^{3+} concentrations. In contrast, Au NP-based thin films that had an intense blue color often had higher Au^{3+} concentration. To standardize the decrease in Au^{3+} concentration between day 0 and day 7 amongst samples, the percentage loss of Au^{3+} was calculated. As shown in Table 7, there was some loss of Au^{3+} over the seven-day period under all three storage solution conditions. The mean percentage loss of [Au^{3+}] indicated that there was no substantial loss of Au NPs from the surface of the substrate over time. This suggested that the significant decrease in contact angle over time in the temporal stability studies with nH_2O was not primarily caused by the desorption of Au NPs.

Table 7. Percentage loss of Au^{3+} on slides from Day 0 to 7 in different storage solutions. Data are reported as mean percentage loss of $[Au^{3+}]$ ± standard deviation, where the mean was calculated from N=3 measurements.

Storage Solution	Mean Percentage Loss of $[Au^{3+}]$ (%)
nH_2O	13 ± 5
nH_2O + 1 mM ascorbic acid	3 ± 3
nH_2O + 1 mM sodium ascorbate	3 ± 3

4. Conclusions and Future Directions

The temporal stability of gold nanoparticle-based thin films was investigated. Thin films were fabricated by a layer-by-layer immersion technique. The following layers were added sequentially on to silicon dioxide glass substrates: APTMS, Au NPs, and DT. Contact angle goniometry was used to assess the presence and the quality of the thin films throughout the fabrication process and the temporal stability studies. The results indicated that gold nanoparticle-based thin films performed better than controls (without Au NPs) over time in nH_2O. However, the greatest decrease in contact angle for both controls and Au NP-containing samples occurred between day 0 and 1. After day 1 a steady decrease in contact angle was observed over the seven-day period. Because the outermost layer of the thin film was very hydrophobic, thin film degradation can be quantified with a decrease in contact angle.

Two possible mechanisms of thin film degradation were explored. The potential desorption of Au NPs from the surface of the thin films was investigated with trace metal analysis. Data gathered from ICP-AES showed that there was a small decrease in Au^{3+} concentration from day 0 to day 7, suggesting that the thin film degradation did not occur primarily by desorption of Au NPs. Another possible mechanism of degradation was the desorption of DT molecules by oxidation. A small concentration of antioxidant (1 mM ascorbic acid or 1 mM sodium ascorbate) was added into the storage solution, nH_2O. In the temporal stability studies, both controls and Au NP-based thin films better retained their integrity over time in comparison to their counterparts in nH_2O. In addition, the decrease in contact angle between day 0 and day 1 was much smaller in comparison to controls and samples that were immersed in just nH_2O. The temporal stability studies with antioxidant suggested that the

oxidation of DT molecules followed by their desorption into the surrounding medium was a mechanism of thin film degradation.

A difference in the time-dependent behavior among controls and samples in storage solutions with and without antioxidant was observed. When thin films were stored in nH_2O, typical temporal stability behavior was characterized by the large initial contact angle drop between days 0 and 1 followed by small decreases and eventual stabilization. In contrast, thin films stored in nH_2O with antioxidant generally experienced moderate decreases in contact angle over the seven-day immersion period, and no stabilization was observed.

Future studies should explore the moderate- to long-term stability of thin films in nH_2O containing antioxidant to see if thin films will reach stabilization. Increasing antioxidant concentration or adding fresh antioxidant into the storage solution between contact angle measurements may allow thin films to reach stabilization faster. Another avenue worth pursuing is the effect of different antioxidants on the temporal stability and degradation of thin films. In addition, more replicates of Au NP-containing samples should be performed to get a better idea of the variability. Additionally, this may aid in reducing the variability. Many applications of thin films involve biological systems. Therefore, further studies could also investigate the time-dependent behavior of a hydrophilic surface as the outermost layer of the thin films.

5. References

1. Plenty of Room at the Bottom. http://www.its.caltech.edu/~feynman/plenty.html (accessed January 19, 2015).
2. Eigler, D. M.; Schweizer, E. K., Positioning single atoms with a scanning tunnelling microscope. *Nature* **1990,** *344* (6266), 524-526.
3. Pelaz, B.; Jaber, S.; de Aberasturi, D. J.; Wulf, V.; Aida, T.; de la Fuente, J. M.; Feldmann, J.; Gaub, H. E.; Josephson, L.; Kagan, C. R.; Kotov, N. A.; Liz-Marzán, L. M.; Mattoussi, H.; Mulvaney, P.; Murray, C. B.; Rogach, A. L.; Weiss, P. S.; Willner, I.; Parak, W. J., The State of Nanoparticle-Based Nanoscience and Biotechnology: Progress, Promises, and Challenges. *ACS Nano* **2012,** *6* (10), 8468-8483.
4. Daniel, M.-C.; Astruc, D., Gold Nanoparticles: Assembly, Supramolecular Chemistry, Quantum-Size-Related Properties, and Applications toward Biology, Catalysis, and Nanotechnology. *Chemical Reviews* **2003,** *104* (1), 293-346.
5. Duchesne, L.; Gentili, D.; Comes-Franchini, M.; Fernig, D. G., Robust Ligand Shells for Biological Applications of Gold Nanoparticles. *Langmuir* **2008,** *24* (23), 13572-13580.
6. Sperling, R. A.; Rivera Gil, P.; Zhang, F.; Zanella, M.; Parak, W. J., Biological applications of gold nanoparticles. *Chemical Society Reviews* **2008,** *37* (9), 1896-1908.
7. Abbas, R. R.; Richardson, T. H.; Hobson, A.; Hassan, A.; Abbas, T. R., Effect of annealing on the surface plasmon resonance of dodecanethiol encapsulated gold nanoparticles Langmuir–Schafer thin films. *Colloids and Surfaces A: Physicochemical and Engineering Aspects* **2014,** *444* (0), 95-103.
8. Rashid, M. H.; Bhattacharjee, R. R.; Mandal, T. K., Organic Ligand-Mediated Synthesis of Shape-Tunable Gold Nanoparticles: An Application of Their Thin Film as Refractive Index Sensors. *The Journal of Physical Chemistry C* **2007,** *111* (27), 9684-9693.
9. Ferhan, A. R.; Guo, L.; Zhou, X.; Chen, P.; Hong, S.; Kim, D.-H., Solid-Phase Colorimetric Sensor Based on Gold Nanoparticle-Loaded Polymer Brushes: Lead Detection as a Case Study. *Analytical Chemistry* **2013,** *85* (8), 4094-4099.
10. Wang, F.; Liu, X.; Lu, C.-H.; Willner, I., Cysteine-Mediated Aggregation of Au Nanoparticles: The Development of a H2O2 Sensor and Oxidase-Based Biosensors. *ACS Nano* **2013,** *7* (8), 7278-7286.
11. Lv, X.; Ge, W.; Li, Q.; Wu, Y.; Jiang, H.; Wang, X., Rapid and Ultrasensitive Electrochemical Detection of Multidrug-Resistant Bacteria Based on Nanostructured Gold Coated ITO Electrode. *ACS Applied Materials & Interfaces* **2014,** *6* (14), 11025-11031.
12. Love, J. C.; Estroff, L. A.; Kriebel, J. K.; Nuzzo, R. G.; Whitesides, G. M., Self-Assembled Monolayers of Thiolates on Metals as a Form of Nanotechnology. *Chemical Reviews* **2005,** *105* (4), 1103-1170.
13. Mamun, A. H. A.; Yoon, S.; Hahn, J. R., Influence of the molecular-scale structures of 1-dodecanethiol and 4-methylbenzenethiol self-assembled monolayers on gold nanoparticles adsorption pattern. *Journal of Colloid and Interface Science* **2014,** *425* (0), 83-90.
14. Pasquarelli, R. M.; Ginley, D. S.; O'Hayre, R., Solution processing of transparent conductors: from flask to film. *Chemical Society Reviews* **2011,** *40* (11), 5406-5441.

15. Malvern Instruments Dynamic Light Scattering: An Introduction in 30 Minutes. http://www.malvern.com/common/downloads/campaign/MRK656-01.pdf (accessed January 20, 2015).
16. van der Zande, B. M. I.; Dhont, J. K. G.; Böhmer, M. R.; Philipse, A. P., Colloidal Dispersions of Gold Rods Characterized by Dynamic Light Scattering and Electrophoresis. *Langmuir* **1999,** *16* (2), 459-464.
17. Mohr, K.; Müller, S. S.; Müller, L. K.; Rusitzka, K.; Gietzen, S.; Frey, H.; Schmidt, M., Evaluation of Multifunctional Liposomes in Human Blood Serum by Light Scattering. *Langmuir* **2014,** *30* (49), 14954-14962.
18. Laure, W.; Woisel, P.; Lyskawa, J., Switching the Wettability of Titanium Surfaces through Diels–Alder Chemistry. *Chemistry of Materials* **2014,** *26* (12), 3771-3780.
19. Brassard, J.-D.; Sarkar, D. K.; Perron, J., Synthesis of Monodisperse Fluorinated Silica Nanoparticles and Their Superhydrophobic Thin Films. *ACS Applied Materials & Interfaces* **2011,** *3* (9), 3583-3588.
20. Baysal, A.; Ozbek, N.; Akman, S., *Determination of Trace Metals in Waste Water and Their Removal Processes*. 2013.
21. Kim, S.; Kang, M.; Kim, S.; Heo, J.-H.; Noh, J. H.; Im, S. H.; Seok, S. I.; Kim, S.-W., Fabrication of CuInTe2 and CuInTe2–xSex Ternary Gradient Quantum Dots and Their Application to Solar Cells. *ACS Nano* **2013,** *7* (6), 4756-4763.
22. Justo, Y.; Sagar, L. K.; Flamee, S.; Zhao, Q.; Vantomme, A.; Hens, Z., Less Is More. Cation Exchange and the Chemistry of the Nanocrystal Surface. *ACS Nano* **2014,** *8* (8), 7948-7957.
23. Bear, A. Surface modification using thin films of gold nanoparticles. Wellesley College, Wellesley College, 2009.
24. Lin, J. Gold Nanopariticle-Based Thin Films on Glass: A Moderate- to Long-Term Stability Study in Aqueous Medium. Wellesley College, Wellesley College, 2007.
25. Worthen, K., Unpublished results. 2012.
26. Flynn, N. T.; Tran, T. N. T.; Cima, M. J.; Langer, R., Long-term stability of self-assembled monolayers in biological media. *Langmuir* **2003,** *19* (26), 10909-10915.
27. Flynn, N. T.; Gewirth, A. A., Attenuation of surface-enhanced Raman spectroscopy response in gold–platinum core-shell nanoparticles. *Journal of Raman Spectroscopy* **2002,** *33* (4), 243-251.
28. Schmid, G., *Metals*. John Wiley & Sons, Inc.: New York, 2001.
29. Abrenica, M. V. A. Surface Functionalization of Gold Nanoparticles for Cancer Therapy. Wellesley College, Wellesley College, 2011.
30. Schmitt, S. G. Fuctionalization of a Multi-Purpose Nanovehicle Platform for Targeted Cancer Therapy. Wellesley College, Wellesley College, 2013.
31. Blatchford, C. G.; Campbell, J. R.; Creighton, J. A., Plasma resonance — enhanced raman scattering by absorbates on gold colloids: The effects of aggregation. *Surface Science* **1982,** *120* (2), 435-455.
32. Song, X.; Zhai, J.; Wang, Y.; Jiang, L., Self-assembly of amino-functionalized monolayers on silicon surfaces and preparation of superhydrophobic surfaces based on alkanoic acid dual layers and surface roughening. *Journal of Colloid and Interface Science* **2006,** *298* (1), 267-273.
33. Kristensen, E. M. E.; Nederberg, F.; Rensmo, H.; Bowden, T.; Hilborn, J.; Siegbahn, H., Photoelectron Spectroscopy Studies of the Functionalization of a Silicon Surface with a

Phosphorylcholine-Terminated Polymer Grafted onto (3-Aminopropyl)trimethoxysilane. *Langmuir* **2006,** *22* (23), 9651-9657.
34. Han, X.; Liu, Y.; Yin, Y., Colorimetric Stress Memory Sensor Based on Disassembly of Gold Nanoparticle Chains. *Nano Letters* **2014,** *14* (5), 2466-2470.
35. Dasog, M.; Scott, R. W. J., Understanding the Oxidative Stability of Gold Monolayer-Protected Clusters in the Presence of Halide Ions under Ambient Conditions. *Langmuir* **2007,** *23* (6), 3381-3387.
36. Hardy, N. J.; Richardson, T. H., Temperature effects on the optical properties of thiol encapsulated gold nanoparticle thin films. *Colloids and Surfaces A: Physicochemical and Engineering Aspects* **2008,** *321* (1–3), 285-291.
37. (a) Chiang, C.-H.; Ishida, H.; Koenig, J. L., The structure of γ-aminopropyltriethoxysilane on glass surfaces. *Journal of Colloid and Interface Science* **1980,** *74* (2), 396-404; (b) Horr, T. J.; Arora, P. S., Determination of the acid-base properties for 3-amino, 3-chloro and 3-mercaptopropyltrimethoxysilane coatings on silica surfaces by XPS. *Colloids and Surfaces A: Physicochemical and Engineering Aspects* **1997,** *126* (2–3), 113-121; (c) Kowalczyk, D.; Slomkowski, S.; Chehimi, M. M.; Delamar, M., Adsorption of aminopropyltriethoxy silane on quartz: an XPS and contact angle measurements study. *International Journal of Adhesion and Adhesives* **1996,** *16* (4), 227-232.

6. Appendix

6.1 Temporal Stability Contact Angles

Table 1-A. Contact angle measurements for thin films in storage solutions with no antioxidant, ascorbic acid, and sodium ascorbate at days 0, 1, 3, 5, and 7. Samples contained Au NPs while controls did not have any Au NPs. Data are reported as mean CA ± 95% CI, where the mean CA was calculated from N=96 CA measurements for control slides and N=48 for sample slides.

Mean Contact Angle (°)						
Storage Solution	nH_2O		nH_2O + 1 mM ascorbic acid		nH_2O + 1 mM sodium ascorbate	
Day	*Control*	*Sample*	*Control*	*Sample*	*Control*	*Sample*
0	66.6 ± 0.8	80 ± 2	71.0 ± 0.5	86 ± 1	68 ± 1	81 ± 2
1	38.5 ± 0.8	62 ± 5	58.0 ± 0.6	78 ± 2	49.8 ± 0.9	73 ± 3
3	30.0 ± 0.8	59 ± 5	48.7 ± 0.9	71 ± 3	42.4 ± 0.9	65 ± 3
5	25.5 ± 0.6	56 ± 5	44.7 ± 0.8	65 ± 2	39.2 ± 0.8	60 ± 3
7	23.5 ± 0.5	55 ± 4	42.6 ± 0.7	61 ± 3	37.2 ± 0.7	56 ± 3